Silicone Wire Embolization-induced Acute Retinal Artery Ischemia and Reperfusion Model in Mouse: Gene Expression Provide Insight into Pathological Processes

Yuedan Wang[a#], Ying Li[a#], Jiaqing Feng[a#], Chuansen Wang[a], Yuwei Wan[a], Bingyang Lv[a], Yinming Li[b], Hao Xie[b], Ting Chen[a], Faxi Wang[b], Ziyue Li[a], Anhuai Yang[a*] & Xuan Xiao[a,b*]

a Department of Ophthalmology, Renmin Hospital of Wuhan University, Wuhan 430060, Hubei, China

b Department of Clinical Laboratory, Institute of Translational Medicine, Renmin Hospital of Wuhan University, Wuhan 430060, Hubei, China

# These authors contributed equally.

*** Correspondence to:** Xuan Xiao, Department of Ophthalmology, Renmin Hospital of Wuhan University, No. 238 Jie Fang Road, Wuhan 430060, Hubei, China. Tel: (86) 027-88041911, Email: xiaoxuan1111@whu.edu.cn

*** Correspondence to:** Anhuai Yang, Department of Ophthalmology, Renmin Hospital of Wuhan University, No. 238 Jie Fang Road, Wuhan 430060, Hubei, China. Email: yah0525@126.com

Abstract

Acute retinal ischemia and ischemia-reperfusion injury are primary causes of retinal neural cell death and vision loss in retinal artery occlusion (RAO). The absence of an accurate mouse model simulating the retinal ischemic process has hampered progress in developing neuroprotective agents for RAO. A unilateral pterygopalatine ophthalmic artery occlusion (UPOAO) mouse model was developed by employing silicone wire embolization combined with carotid artery ligation. The survival of retinal ganglion cells and visual function were evaluated to determine ischemia duration. Immunofluorescence staining, optical coherence tomography, and hematoxylin and eosin staining were utilized to assess changes in major classes of neural cells and retinal structure degeneration at two reperfusion durations. Transcriptomics was employed to investigate alterations in the pathological process of UPOAO following ischemia and reperfusion, highlighting transcriptomic differences between UPOAO and other retinal ischemia-reperfusion models. The UPOAO model successfully replicated the acute interruption of retinal blood supply seen in RAO. 60-minute ischemia was confirmed to lead the major retinal neural cells loss and visual function impairment. Notable thinning of the inner layer of the retina, especially the ganglion cell layer, was evident post-UPOAO. Temporal transcriptome analysis revealed various pathophysiological processes related to immune cell migration, oxidative stress, and immune inflammation during non-reperfusion and reperfusion periods. The resident microglia within the retina and peripheral leukocytes which access to the retina were pronounced increased on reperfusion periods. Comparison of differentially expressed genes between the UPOAO and high intraocular pressure models

identified specific enrichments in lipid and steroid metabolism-related genes in the UPOAO model. The UPOAO model emerges as a novel tool for the screening of pathogenic genes, promoting further therapeutic research in RAO.

Key words: Retinal artery occlusion; Mouse model; Ischemia and reperfusion injury; Transcriptomics; Immune cell

1 Introduction

Retinal artery occlusion (RAO) is a severe ophthalmic disease characterized by a sudden interruption of blood flow in the retinal artery, leading to retinal ischemia [1]. More than 60% of RAO patients experience impaired vision, ranging from finger counting to complete vision loss [2]. RAO patients face an elevated risk of cardiovascular and cerebrovascular events [3-5]. Retinal ischemia and hypoxia can cause irreversible damage to retinal cells in 90 minutes [6]. This damage is possibly attributed to the continued apoptosis of retinal ganglion cells (RGCs), triggered by inflammation and oxidative stress. Unfortunately, conservative treatments for RAO, such as eye massage and hyperbaric oxygen therapy, offer limited therapeutic benefits [7]. Thrombolysis, though effective, is also restricted by the narrow treatment time window (often within 4.5 hours) [8]. However, when blood flow is restored to the ischemic area after thrombolysis, it can cause a sudden elevation of tissue oxidative levels, resulting in ischemia-reperfusion injury (IRI) in the retina [9]. IRI is a common pathological condition that can trigger inflammation, retinal tissue injury and visual impairment [10]. Therefore, to comprehensively investigate the pathophysiological changes and explore potential neuroprotective therapeutics after retinal ischemia and

reperfusion, it is of paramount importance to develop an animal model that can accurately simulate the pathological processes of RAO.

Various animal models have been employed to investigate the effects of retinal injury resulting from ischemia and subsequent reperfusion in RAO [6, 11, 12]. Based on the methods used for modeling, retinal ischemia-reperfusion models can be categorized into two groups: 1) Intravascular occlusion models, including photochemical-induced thrombosis model and vascular intervention model; 2) Extravascular occlusion models, including central retinal artery ligation (CRAL) model, unilateral common carotid artery occlusion (UCCAO) model, and high intraocular pressure (HIOP) model. The photochemical-induced thrombosis model and vascular intervention model have been reported as useful tools to assess retinal injury after ischemia and reperfusion. However, both models are limited by the need for trained interventional radiologists and high technique [13, 14]. CRAL, which directly clips or ligates the central retinal artery, also presents its drawbacks. This model may cause optic nerve damage, and it is difficult to apply in small animals like mice, which limits its use in experiments with larger sample sizes [6]. UCCAO, a retinal hypoperfusion model induced by occlusion of the unilateral common carotid artery (CCA), is better at simulating chronic ischemic retinal disease rather than acute retinal ischemia [15, 16]. The HIOP model is a widely utilized mouse model for studying ischemia-reperfusion in acute primary angle-closure glaucoma (APACG) [17]. However, it is worth noting that the mechanical compression of the retina caused by saline injection may also lead to retinal damage, potentially influencing IRI

research. Therefore, it is critically important to develop a simple and low-skill-required mouse model that can simulate the acute retinal ischemia and reperfusion injury in RAO patients.

To better simulate the retinal ischemic process and possible IRI following RAO, we developed a novel vascular-associated mouse model called unilateral pterygopalatine ophthalmic artery occlusion (UPOAO) model. In this model, we employed silicone wire embolization and carotid artery ligation to completely block the blood supply to the retina. We characterized the major classes of retinal neural cells and evaluated visual function following different durations of ischemia (30 minutes and 60 minutes) and reperfusion (3 days and 7 days) after UPOAO. Additionally, we utilized transcriptomics to investigate the transcriptional changes and elucidate changes in the pathophysiological process of the UPOAO model after ischemia and reperfusion. Lastly, we underscored the transcriptomic differences between the model and other retinal ischemic-reperfusion models, including HIOP and UCCAO, and revealed its unique pathological processes similar to that of retinal IRI in RAO. The UPOAO model offers new insights into the mechanisms and pathways involved in ischemia and reperfusion studies of RAO, providing a foundation for studying the protective strategy for ocular ischemic diseases.

2 Methods and materials

2.1 Animals

Eight-week-old male C57BL/6 mice were used in the experiments. Only male mice were

used to exclude the potential influence of estrogenic hormones. The mice were provided with sufficient food and water and were maintained on a 12-hour dark-light cycle in a room with regulated temperature conditions. All experimental procedures were designed and conducted according to the ethical guidelines outlined in the ARVO Statement for the Use of Animals in Ophthalmic and Vision Research. The study protocol and methods received approval from the Experimental Animal Ethics Committee of Renmin Hospital of Wuhan University (approval number: WDRM-20220305A).

2.2 Preparation work and surgical procedure of UPOAO model

Eight-week-old male C57BL/6 mice weighing 20-25 grams were used in this study. An isoflurane-based anesthesia system was prepared to induce and maintain general anesthesia in mice during surgical procedures. The mice were anesthetized with a 1.5-2% concentration of isoflurane delivered in a mixture of nitrous oxide and oxygen via rubber tubing. Body temperature was maintained at 37±0.5°C throughout the surgery. Surgical instruments were sterilized with 75% ethanol before use to ensure sterility.

The mouse was gently positioned in a supine posture on a heating blanket and its neck was exposed. The preparation involved depilation of the neck area, followed by skin disinfection, and finally, a midline incision along the neck was made. Following the neck gland separation with two tweezers, a careful blunt dissection was employed to separate the left CCA, internal carotid artery (ICA) and external carotid artery (ECA), avoiding compression of nearby nerves and veins (**Fig 1A**) (**Video 1**). Then, the CCA and ICA were

ligated with a 6-0 suture. Secure a knot using a 6-0 suture at the distal end of ECA and create a slipknot at the proximal end (**Fig 1B**). Utilize an ophthalmic scissor to create a small inverted “V”-shaped incision between the two suture knots on the ECA. Insert a specialized silicone wire embolus of which length is 7±0.1 mm and diameter is 0.19±0.1 mm through the incision, directing it into the ECA and further into the CCA (**Fig 1C**). Next, the ligation on the ICA was removed, and the ECA was cut at the point where the artery had been previously incised with scissors. Subsequently, the silicone wire embolus was retracted to the bifurcation of the CCA, rotated counterclockwise and inserted into the ICA and further into the pterygopalatine artery (PPA) (**Fig 1D1**). The silicone tail of the silicone wire embolus was near the bifurcation of CCA (**Fig 1D2**), effectively obstructing the ophthalmic artery (OA) (**Video 2**). Then fasten the slipknot and suture the skin. The mouse was free to move around during arterial embolization.

Following a predetermined ischemia embolization time, the silicone wire embolus was carefully removed from the PPA without massive hemorrhage (**Fig 1E**). The CCA suture was removed and the arterial reperfusion was restored (**Fig 1F**) (**Video 3**). Then suture the skin wound and routinely feed mice during reperfusion (**Fig 1G**).

2.3 Staining of retinal vessels

To clearly visualize the retinal vessels, rhodamine-labeled canavalin A was used for mouse heart perfusion. The mouse was anesthetized by 1% sodium pentobarbital and placed in a supine position on a foam board resting on a tray. The mouse’s sternum was

opened, exposing the heart. A needle attached to the perfusion tube was inserted into the left ventricle via the apex of the mouse heart and fixed. The right atrial appendage of the mouse was dissected with scissors to allow blood outflow. Saline solution was perfused through the left ventricle using a pump system to drain the blood from arteries. Subsequently, prepared solution of rhodamine labeled canavalin A was injected into the mice and circulated throughout the mouse vessels for 30 minutes. The mice were sacrificed and their eyes were extracted and immersed in PFA for one hour in the dark. Obtain a flat-mounted retina and capture retinal images using the Leica SP8 confocal microscope equipped with a 10× objective.

2.4 Quantification of RGCs and microglia

The mice were euthanized by cervical dislocation and their eyes were fixed in 4% paraformaldehyde (PFA) for 60 minutes at room temperature (RT). Subsequently, the cornea and lense were excised, and the retina was isolated intact to perform retinal flat-mounting. The retina was immersed in PBS with 5% Bovine Serum Albumin (BSA) and 0.5% Triton X-100 for overnight blocking and then incubated with Brn3a antibody (Santa Cruz Biotechnology, Dallas, Texas, USA) or Iba1 antibody (Wako, Japan). Following a two-day incubation with the primary antibody, the retina was gently washed three times with PBS. Subsequently, the retina was incubated with Alexa Fluor 594 (AntGene, Wuhan, China) in a light-protected cassette for two days. After three rinses, the retina was uniformly sectioned into a four-leaf clover morphology and flattened using a coverslip. Finally, retinal flat-mounts labeled with Brn3a were imaged using the Leica SP8

confocal microscope (Leica TCS SP8, Germany) equipped with 20× objective, while those labeled with Iba1 were imaged utilizing a fluorescence microscope (BX63; Olympus, Tokyo, Japan). Each quadrant was consistently subdivided into central, middle and peripheral fields at regular intervals. The surviving RGCs and activated microglia were quantified and averaged using Image-J software (National Institutes of Health, USA).

2.5 Electroretinogram (ERG)

Mice were dark-adapted overnight before ERG and all subsequent procedures were carried out in the dark environment. Before ERG, mice were anesthetized by 1% sodium pentobarbital through intraperitoneal injection and their pupils were dilated. A subcutaneous electrode was inserted into the posterior cervical skin, a tail electrode was affixed to the posterior end of the mouse tail, and the corneal electrode was gently placed on the central corneal surface. The RetiMINER-C visual electrophysiological system (3VMED Co., Ltd., Shanghai, China) was employed for recording electrical responses. The a-waves, b-waves, and Oscillatory Potentials (OPs)-waves after flash stimuli of 0.01, 0.03, 0.1, 0.3, 1.0, 3.0, and 10.0 cd.s/m^2 in scotopic adaptation were recorded. The amplitudes and implicit times of a-waves, b-waves and OPs-waves in response to various flash stimuli were analyzed.

2.6 Optical Coherence Tomography Imaging (OCT) and Fluorescein Fundus Angiography (FFA)

The mice were placed on the platform of a Spectralis HRA+OCT device (Heidelberg

Engineering, Heidelberg, Germany) for OCT imaging following anesthesia. Pupil dilation was performed, and normal saline was applied regularly to maintain corneal moisture in the mice. The focal length of the device was adjusted so that the mouse retina was clearly visible. Mouse's head was gently repositioned to take pictures of the peripheral fundus. Multi-line mode was used to scan each layer of the retina and four-quadrant fields of view centered on the nipple on the upper left, lower left, upper right, and lower right were recorded. In this study, IMRL (inner middle retina layer) was defined as the combined thickness of the retinal nerve fiber layer (RNFL), ganglion cell layer (GCL), and the inner plexiform layer (IPL). MRL (middle retina layer) was defined as the combined thickness of the inner nuclear layer (INL) and the outer plexiform layer (OPL). ORL (outer retina layer) was defined as the combined thickness of the rest to the retinal pigment epithelium (RPE). Total retinal thickness (TRT) of the sensory retina was manually segmented and encompassed the entire thickness from the nerve fiber layer to the photoreceptor layer. The thickness of retina at 1.5 papillary diameters (PD), 3.0 PD, and 4.5 PD from the center of the optic disc were measured using the Heidelberg measuring tool.

For FFA, mice were anesthetized and their pupils were also dilated. Subsequently, fundus angiography was recorded immediately following intraperitoneal injection of sodium fluorescein (for no longer than 5 seconds), with photos taken alternately for both eyes.

2.7 Hematoxylin and eosin (HE)

Mouse eyes were fixed in FAS eyeball fixation solution (Service-bio, Wuhan, China) for 48

hours, followed by dehydration and subsequent embedding in paraffin. Paraffin was trimmed parallel to the optic nerve to obtain 3-4 μm thick sections where the optic nerve was located. Six paraffin sections from each eyeball were stained with HE. The Olympus fluorescence microscope was employed for taking pictures. Retinal thickness within 500 μm of the optic disc was measured using the Image-Pro Plus 6.0 software.

2.8 Staining of Retinal Sections

For immunofluorescence, mouse eyes were fixed in 4% PFA solution and subjected to gradient dehydration using 10%, 20%, and 30% sucrose solutions. The following day, the eyes were embedded in optimum cutting temperature (OCT.) compound (SAKURA, American) and frozen at -80°C. Several 14-μm-thick frozen sections were obtained from each eyeball through the frozen microtome (Leica, Wetzlar, Germany). The section surface was parallel to the optic nerve, and 3-6 frozen sections were mounted on a single slide. The slides were stored at -20°C until use.

All sections were blocked with 5% BSA and 0.5% Triton X-100 in PBS for 2 hours. Primary antibodies, as listed in **Table 1**, were diluted in PBS containing 5% BSA and 0.5% Triton X-100 and incubated at 4°C overnight. The following day, after three rinses, the sections were incubated with the second antibodies at RT for 2 hours in a cassette, followed by three washes. And then sections were stained with DAPI (Service-bio, Wuhan, China) for 15 minutes. After the final three rinses, the frozen sections were sealed. A Leica SP8 equipped with 40× objective was used to photograph frozen sections near the optic nerve

head. The fluorescence intensity of all slices of each eye was mounted using Image-J.

2.9 Surgical procedure of UCCAO model and HIOP model

Animals for UCCAO were prepared and managed as described in the UPOAO model procedure. After blunt dissection, the left CCA was ligated by a 6-0 suture. After 60 minutesligation, the suture was removed and the skin wound was subsequently closed with sutures. Mice were routinely fed during reperfusion and mouse retinas of UCCAO were harvested 7 days post-surgery.

HIOP model was performed based on previous methods [18]. Briefly, mice were anesthetized by intraperitoneal injection of 1% sodium pentobarbital. Mice pupils were dilated using Tropicamide Phenylephrine Eye Drops (0.5% tropicamide and 0.5% deoxyadrenaline hydrochloride, Santen Pharmaceutical) 5 minutes in advance. An insulin hypodermic needle, attached to a silicone elastomer tube, was inserted into the anterior chamber of the unilateral experimental eye. Elevate intraocular pressure (IOP) for 60 minutes by raising the height of the saline solution storage bag to 162 cm and remove the needle to immediately restore IOP to baseline levels. Iris whitening and loss of retinal red-light reflexes demonstrated retinal ischemia. After surgery, levofloxacin hydrochloride ophthalmic gel was applied to the eyes of mice. Mouse retinas of HIOP were collected 7 days post-surgery.

2.10 Transcriptome sequence and analysis

Retinal samples from UPOAO, HIOP, and UCCAO mice were extracted and promptly frozen in liquid nitrogen within 10 minutes of cervical dislocation. Total RNA extraction followed the protocol outlined in the TRIzol Reagent manual (Life Technologies, CA, USA). RNA integrity and concentration were assessed using an Agilent 2,100 Bioanalyzer (Agilent Technologies, Inc, Santa Clara, CA, USA). The resulting RNA samples were then pooled and subjected to sequencing on the Illumina HiSeq3000 platform in a 150-bp paired-end read format. Raw RNA-sequencing (RNA-seq) reads underwent preprocessing and quantification using the featureCounts function in the SubReads package version 1.5.3, with default parameters.

RNA-seq analysis was repeated across 5 mice in the no-perfusion group, 4 mice in the 3-day perfusion group, and 5 mice in the 7-day perfusion group of the UPOAO model. Additionally, retinas from both the 7-day HIOP experimental eyes and UCCAO bilateral eyes were collected (n=5) for analysis.

Data normalization and subsequent processing utilized the 'limma' package in R software (version 4.2.3) [19]. For visualization purposes, volcano plots and Venn diagrams were generated to identify significant differential expression genes (DEGs) and perform Gene Ontology (GO) annotation analysis. DEGs with |log2 fold change (FC)| >1 and adjusted p-value <0.05 were deemed statistically significant. Enrichment analysis focused on DEGs with an adjusted $p < 0.05$ and an enriched gene count >5. To visualize the expression patterns of significant DEGs, a heatmap was generated using the 'pheatmap'

package. Gene Set Enrichment Analysis (GSEA) was conducted using the GSEA program (version 4.3.2) [20], employing the default gene set m-subset (mh.all.v2023.1.mm.symbols.gmt) to explore significant functional and pathway differences. Enriched pathways were classified based on criteria such as adjusted p-value (<0.05), False Discovery Rate (FDR) q-value (<0.25), and normalized enrichment score (|NES| > 1). Furthermore, protein-protein interaction (PPI) analysis was performed using the Search Tool for the Retrieval of Interacting Genes (STRING) database (https://string-db.org/) [21]. Genes showing a higher degree of protein-level interactions with others were further analyzed using Cytoscape software (version 3.8.2) to generate a downstream PPI map. The resulting PPI pairings with an interaction score > 0.7 were extracted and visualized using Cytoscape 3.9.0 [22].

2.11 Real-time Quantitative polymerase chain reaction (RT-qPCR)

RNA was extracted from fresh mouse retinal samples and subjected to reverse transcription using HiScript lll RT SuperMix for qPCR (Vazyme, China) following the manufacturer's instructions. RT-qPCR analysis was conducted on a CFX instrument (Bio-rad) using AceQ qPCR SYBR Green Master Mix (Vazyme, China). The PCR program comprised 40 cycles of 10 seconds at 95℃ and 30 seconds at 60℃. Assays were performed in triplicate, and Ct values were normalized to beta actin levels. Relative quantification of target gene expression was performed using the 2-ΔΔCt method. Primer details are provided in **Table S1**.

2.12 Statistical Analysis

All data were analyzed using GraphPad Prism version 9.0 (GraphPad Software, San Diego, CA, USA). Each experimental group included a minimum of three biological replicates. T-tests were employed for comparing two groups, including RGCs and microglia counting, Ops-waves analysis, retinal thickness measurements in HE staining, and fluorescence intensity quantification. Two-way ANOVA (two-way analysis of variance) test was used for more than two different experimental groups, including ERG waves and retinal thickness measurements in OCT. All data were presented as the mean ± standard error of the mean (s.e.m) and the statistical graphs were depicted as scatter bar graphs and line charts. $P < 0.05$ was considered statistically significant.

3 Results

3.1 Silicone wire embolus insertion interrupts retinal blood flow

To reproduce the retinal ischemic process and potential IRI in RAO, we established a mouse model of UPOAO by combining silicone wire embolization and ligation of the carotid artery. Model validation was conducted through a series of experiments, with detailed descriptions provided in the Materials and Methods (**Fig. 1A-G**). To confirm blood flow disruption, fluorescently labeled lectin cardiac perfusion and FFA were performed. Rhodamine-labeled canavalin A was perfused with the silicone wire embolus in vivo, and bilateral eyes were evaluated. The sham eye exhibited normal blood perfusion in the retina, while the experimental eye showed no perfusion (**Fig. 1H, I**). FFA revealed delayed and limited perfusion in the experimental lateral retina, primarily near the optic disc (**Fig.**

1J, K). These findings indicate that insertion of the silicone wire embolus resulted in impaired blood flow to the retina.

3.2 60-minute ischemia in UPOAO damage retinal structure and function

To investigate the optimal ischemic duration, mice underwent two ischemic periods: 30 and 60 minutes, followed by reperfusion periods of 3 and 7 days. Retinal structure and visual function were assessed through flat-mounted retina analysis and flash electroretinography (ERG).

In the 30-minute ischemia group, no significant RGCs death was observed after 3 days (**Fig. 2A, B**) or 7 days of reperfusion (**Fig. 2C, D**). However, with 60 minutes of ischemia and 3 or 7 days of reperfusion, reductions in RGC density were evident (**Fig. 2E-H**). ERG results showed no statistical difference in amplitudes between bilateral eyes after 3 and 7 days of 30-minute reperfusion (**Fig. 3A-C**). However, the b-wave amplitude notably declined after 60 minutes of ischemia and 3 days of reperfusion (**Fig. 3D**). By 7 days of reperfusion, the b-wave amplitude had halved compared to sham eyes (**Fig. 3E**). The appearance time of the a-wave and b-wave in the experimental and control eyes was consistent within each of the four groups (**Fig. S1**). Additionally, the amplitudes of OPs in the experimental eyes, particularly in the 60-minute ischemia and 7-day reperfusion group, significantly decreased to less than 50% of those in the sham eyes (**Fig. 3F, G**). Based on RGCs survival and changes in ERG waves, we determined that a 60-minute ischemic duration is optimal for the UPOAO model.

3.3 Evaluation of retinal thickness in UPOAO through OCT and HE

To assess retinal thickness non-invasively in the UPOAO model, we conducted OCT imaging during 3-day and 7-day reperfusion periods. Due to the challenge of distinguishing the RNFL, GCL, and IPL in OCT images, we utilized the IMRL to represent the cumulative thickness of these layers. Similarly, the MRL represented the INL and OPL, while the ORL encompassed the region from the inner segment/outer segment (IS/OS) to the RPE. Following a 3-day reperfusion period, no significant changes were observed in IMRL, MRL, and ORL at distances of 1.5, 3, and 4.5 PD from the optic disc (**Fig. 4B, Fig. S2A, B**). However, total retinal thickness decreased at a distance of 4.5 PD (**Fig. 4C**). After 7 days of reperfusion, total retinal thickness decreased at distances of 1.5 PD, 3 PD, and 4.5 PD, primarily due to inner retinal thinning (**Fig. 4D-F, Fig. S2C, D**).

For a detailed analysis of inner retinal thickness, we extracted UPOAO mouse eyes and stained them with HE. The thickness of RNFL + GCL increased at 3 days of reperfusion (**Fig. 4H**), followed by a decrease at 7 days of reperfusion (**Fig. 4L**). IPL thickness decreased at both 3 days and 7 days of reperfusion (**Fig. 4I, M**), while INL thickness decreased only at 7 days of reperfusion (**Fig. 4N**). We hypothesized that the initial swelling of GCL in response to acute ischemia and hypoxia led to early thickening, followed by gradual thinning due to tissue dysfunction. This hypothesis was supported by the observation of RGC loss and reduced IMRL thickness evaluated by OCT at 7 days (**Fig. 4E**).

We observed that changes in retinal thickness became noticeable at 3 days post-UPOAO and exhibited a significant decrease at 7 days, as observed in OCT. HE results further elucidated that alterations in inner retinal thickness constituted a substantial portion of the total retinal thickness during the early reperfusion stage after UPOAO.

3.4 Survival of retinal neural cells in UPOAO

Given that mouse retinal function heavily relies on rod cells, and scotopic (low light) vision is primarily governed by rod photoreceptors, the observed reductions in b-wave and OPs-wave amplitudes indicate impaired synaptic transmission within the inner retina [23]. Our OCT and HE findings suggest structural injuries within the inner retina. Notably, a-waves in ERG and the thickness of the outer retinal layers in both OCT and HE remained unchanged. To delve deeper into these observations, we conducted immunofluorescence staining to investigate alterations in major retinal cell types, primarily focusing on Bipolar cells (BCs), photoreceptor cells, Horizontal cells (HCs), cholinergic amacrine cells.

3.4.1 BCs loss and photoreceptor cells survival

PKCα is a marker that delineates BCs, with their cell bodies primarily located in the outermost part of the INL, axonal terminals extending into the innermost part of the IPL, and dendrites confined to the OPL (**Fig 5A, B**). In the experimental UPOAO eyes, BCs did not show significant changes at the 3-day reperfusion mark but exhibited dramatic alterations by the 7-day reperfusion period (**Fig 5A2, B2**). Particularly, the immunostaining

density of BCs' dendritic and axonal arbors notably decreased at the 7-day reperfusion mark. BCs account for approximately 40% of INL cells in mice, and their somata and axonal processes form a substantial part of the INL and IPL, consistent with the thinning of the INL observed in both OCT and HE at 7 days (**Fig 4E, N**). It's noteworthy that the decline in PKCα+ BCs at the 7-day reperfusion point coincided with the decrease in b-wave amplitude in ERG (**Fig 3E**), indicating the functional interplay between BCs and other cells.

Recoverin marks the somata and outer segments of photoreceptor cells and is localized within the outer nuclear layer (ONL) (**Fig S3A, B**). Interestingly, recoverin-positive photoreceptors remained relatively stable throughout the reperfusion periods, which aligns with the a-waves observed in ERG (**Fig 3D, E**) and the changes seen in the outer retinal layers in OCT (**Fig S2C, D**).

3.4.2 HCs and cholinergic amacrine cells loss

We proceeded to evaluate HCs and cholinergic amacrine cells using calbindin and ChAT immunostaining, respectively. Calbindin immunostaining delineated the somata of HCs within the INL, with their terminal axon connections linearly positioned within the OPL (**Fig 5E, F**). In the UPOAO experimental eyes, a notable reduction in HCs number was observed at both 3-day and 7-day reperfusion periods. By 7 days, a significant decrease in cell body numbers, a considerable reduction in axon density, and disrupted linear connections were evident (**Fig 5F2**).

ChAT$^+$ cell bodies located in the GCL and INL, with dendrites forming two narrow stratified bands within the IPL. The immunofluorescence density of ChAT$^+$ amacrine cells decreased notably after 3 days and even more prominently after 7 days (**Fig 5I, J**). The fluorescence intensity of the two bands within the IPL markedly weakened and was nearly invisible by 7 days (**Fig 5J2**).

3.5 Time course transcriptome analysis revealed features of different reperfusion periods in UPOAO

To explore the pathophysiological processes of UPOAO, we extracted retinas of bilateral eyes for transcriptome sequencing. The samples encompassed the 60-minute ischemic eyes without reperfusion, 60-minute ischemia followed by 3-day reperfusion, 60-minute ischemia followed by 7-day reperfusion, which were compared to the sham eye as controls.

In the no-perfusion group, 215 genes were upregulated and 204 genes were downregulated (**Fig 6A**). GO enrichment analysis revealed that DEGs were related to leukocyte migration, epidermis development, myeloid leukocyte migration and other cell migration pathways (**Fig 6B**). The heatmap showed the upregulated and downregulated genes of immune cells migration-related pathways at the no-perfusion period in UPOAO (**Fig 6C**) and high-connectivity DEGs (‘hub genes’) were also enriched in these pathways, such as Dusp1 and Fos (**Fig S4A**). GSEA also showed similar results (**Fig S4B-D**). These

results suggested early ischemic processions such as cell migration and potential collateral vessel formation.

In the 3-day reperfusion group, 372 genes were upregulated and 170 genes were downregulated (**Fig 6D**). GO enrichment analysis revealed that 3-day reperfusion DEGs were related to energy metabolism, mitochondrial regulation, and oxidative stress pathways (**Fig 6E**). The heatmap showed the upregulated and downregulated genes of oxidative stress-related pathways at 3-day reperfusion in UPOAO and some hub genes, such as Mrpl18 and Mrps23, were included in the heatmap (**Fig 6F, Fig S5A)**. GSEA showed the pathway of bounding membrane of organelle, cell surface and plasma membrane protein complex changed (**Fig S5B**). Furthermore, 44 overlapping genes, between mitochondrial genes and DEGs of 3 days post-UPOAO, mainly related to mitochondrial transport and the mitochondrial tricarboxylic acid cycle (**Fig S5C, D**). These results suggested mitochondria and metabolism were involved in IRI.

In the 7-day reperfusion group, 429 genes were upregulated and 310 genes were downregulated (**Fig 6G**). The 7-day reperfusion DEGs were enriched in regulation of immune effector process, positive regulation of response to external stimulus and inflammation (**Fig 6H**). The heatmap showed the upregulated and downregulated genes of immune inflammation-related pathways at 7-day reperfusion in UPOAO and most hub genes were also enriched in this pathway, such as Cd86, Cd48 , Tlr4, Tlr6 (**Fig 6I, Fig S6A**). GSEA also showed similar results (**Fig S6B**). What’s else, RT-qPCR confirmed the

immune inflammation-related gene expression was upregulated (**Fig S8**). Significantly, 112 overlapping genes, between the immune-related genes and DEGs at 7 days post-UPOAO, mainly pertain to immune receptor activity, phagocytic vesicle, etc. (**Fig S6C, D**). These results underscore the predominant role of immune responses during this stage.

To explore the association between 3-d reperfusion and 7-d reperfusion changes, we analyzed the DEGs and found 17 overlapping genes (**Fig S7A**), mainly associated with the nitric oxide biosynthetic process (**Fig S7B**). Our finding indicated that the immune inflammatory response observed after 7 days of reperfusion may be the cumulative effect of the acute oxidative stress response during the initial 3-day reperfusion period.

3.6 Leukocytes Infiltration and Microglial Activation

Time course transcriptome analysis underscore the predominant role of immune inflammatory responses during the reperfusion stage. Since the inflammatory response in RIRI has been reported was orchestrated by peripheral immune cells and resident immune cells within the retina [24, 25], we demonstrated the presence of leukocyte infiltration and microglial activation in UPOAO model. Immunofluorescent staining for CD45 was performed on retinas at different time points post-modeling to visualize the distribution and quantity of white blood cells (**Fig 7A-D**). Laser confocal Z-plane projections confirmed minimal leukocyte infiltration in the retinas of sham eyes, which showed $CD45^+$ cells at the vascular lumen likely representing patrolling cells (**Fig 7A**). A

significant increase in $CD45^+$ cells was observed in UPOAO model retinas at 1 day (**Fig 7E**), with a progressive increase in quantity over time (**Fig 7F, G**). Notably, the majority of $CD45^+$ cells in UPOAO model retinas at 1 day displayed a morphology similar to that of vascular leukocytes (**Fig 7B**), suggesting a large influx of peripheral white blood cells into the retinal tissue. In contrast, $CD45^+$ cells at 3-day and 7-day reperfusion exhibited a combination of amoeboid and branched morphologies (**Fig 7C, D**), indicative of activated states.

Microglia, known to undergo activation and morphological changes in response to various insults, were examined in the superficial retina of sham and UPOAO eyes. Immunofluorescent staining for Iba1 was conducted on flat-mounted retinas at 3-day and 7-day post-reperfusion. In sham eyes, $Iba1^+$ microglia displayed small soma and elongated dendrites, evenly distributed within the retina (**Fig 7H1, I1**). Conversely, UPOAO retinas exhibited numerous activated $Iba1^+$ microglia with enlarged soma, shortened dendrites, and an ameboid appearance (**Fig 7H2, I2**). The number of $Iba1^+$ microglia in UPOAO retinas was approximately five times higher than that in sham eyes at 3 days (**Fig 7J**), with a further increase observed at 7 days (**Fig 7K**), albeit less prominent compared to the 3-day time point (**Fig 7J**). The results indicated a potential reduction in immune-mediated inflammation over time.

3.7 RNA-seq comparison between UPOAO and extravascular occlusion models

The transcriptome of two extravascular occlusion models HIOP and UCCAO were

analyzed for a further study of the characteristics of UPOAO. The HIOP model induces ischemia through anterior chamber perfusion with normal saline (**Fig 8A**), while the UCCAO model involves ligation of the unilateral common carotid artery (**Fig 8H**). RNA-seq analysis of retinas exposed to 60 minutes of ischemia followed by 7-day reperfusion in the HIOP model revealed enrichment in immune-related pathways, specifically highlighting increased activity in leukocyte-mediated immunity and regulation of immune effector processes (**Fig 8B**). This finding was consistent with GO analysis, which showed associations with toll-like receptor binding, T cell receptor binding processes, and immune-related functions in the overlapping DEGs between HIOP and UPOAO models (**Fig 8C, D**). To delve deeper, we explored the remaining DEGs in the HIOP model in addition to the overlapping genes. GO analysis revealed that the remaining DEGs in the HIOP model were also enriched in immune responses, such as the T cell receptor complex pathway, adaptive immune response, and B cell-mediated immunity function (**Fig 8E**). Remarkably, upon examining the remaining DEGs specific to the UPOAO model, GO analysis showed DEGs distinctly related to lipid and steroid metabolic processes (**Fig 8F, G**). This observation indicates that the UPOAO model, closely related to RAO, not only exhibits conventional immune responses but also likely involves unique regulation of lipid and steroid metabolism.

Similarly, the UCCAO model exhibited associations with negative regulation of B cell proliferation, lymphocyte activation, and related processes (**Fig 8I**). Additionally, hub genes identified through protein-protein interaction (PPI) analysis were presented (**Fig 8J**). However, the UCCAO model displayed minimal overlap with the UPOAO model, with only

15 overlapping DEGs identified in the Venn diagram analysis (**Fig 8K**). Further analysis of the UCCAO DEGs highlighted two genes (Mettl14 and YTHDF2) related to m6A modifications (**Fig 8L**). Although both UPOAO and UCCAO models occludes arterial blood flow, our results revealed that the pathophysiological processes of two models were particularly different in 7-day reperfusion.

4 Discussion

This study aimed to develop a more appropriate mouse model for investigating the ischemia-reperfusion process in RAO and unravelling the underlying pathophysiological mechanisms. We combined silicone wire embolization with carotid artery ligation and effectively blocked the blood supply to the retina artery, which closely mimics the characteristics of the acute interruption of blood supply in RAO patients [26]. In the UPOAO model, a 60-minute period of ischemia time could simulate the injury of the major retinal neural cells like RGCs, BCs, HCs, cholinergic amacrine cells, and the resultant visual impairment. Moreover, histologic examination demonstrated thinning of the inner layer of the retina, especially the GCL layer. Time course transcriptome analysis revealed various pathophysiological processes related to immune cell migration, oxidative stress, and immune inflammation during non-reperfusion and reperfusion periods. The resident microglia within the retina and peripheral leukocytes which access to the retina were pronounced increased on reperfusion periods. Additionally, we compared the transcriptomic signatures of the UPOAO model with two commonly used ischemia-reperfusion mouse models (HIOP and UCCAO), shedding light on the potential

relevance of the UPOAO model to ocular vascular occlusive diseases.

The UPOAO mouse model can effectively simulate the characteristic features of RAO as observed in patients. RAO patients often exhibit distinctive patterns in dark ERGs, where b-waves are reduced while a-waves remain stable [27-29]. In our study, we observed the same phenomenon in ERG amplitude after 60-minute ischemia in the UPOAO model. This was further confirmed by immunofluorescence staining of bipolar cells and photoreceptor cells. Importantly, a previous study has linked the thinning of the inner retina with alterations of ERG in patients with RAO [30]. Our result showed that ischemic damage predominantly affected the inner layer of the retina, while the outer layer was almost unaffected. This distinction is attributed to the inner layer's reliance on the retinal artery for blood supply while the outer layer is supplied by the choroid. Additionally, histological examination revealed increased thickness of retinal NFL and GCL layers, as well as decreased thickness of the IPL at 3-day reperfusion, indicating that ischemia-induced edema has not completely subsided.

This study comprehensively explored the transcriptomic signature after ischemia and revealed resident and peripheral Immune cells may play a major role in pathological processes. We uncovered that in the non-reperfusion group, the transcriptional changes are primarily involved in immune cells such as leukocytes, neutrophils migration from the blood vessels into the ischemic retinal tissue. This process is closely linked to the injury during ischemia and reperfusion, where leukocytes and neutrophils infiltrate into the

neural tissue through the vascular endothelium [31, 32]. Our results showed increased $CD45^+$ leukocytes in retina and retinal microvascular, suggesting that the leukocytes were recruited form the bloodstream to the damaged retinal tissue following reperfusion period. During the process of leukocytes access to the retina, chemokines, chemokine receptors, adhesion molecules and components of the cytoskeleton play an important role in regulating endothelial permeability and facilitating the adhesion of leukocytes to endothelial cells [33, 34], which is consistent with our findings of related genes.

Moving on to the 3-day reperfusion period, we observed an increased number of DEGs significantly involved in the critical pathological response of oxidative stress in the context of IR tissues. The generation of reactive oxygen species (ROS) in mitochondria and subsequent oxidative stress are widely recognized as major causes of retinal cell damage induced by IR [35, 36]. This suggests that mitochondrial function, which is involved in oxidative stress processes, may play an important role in the pathophysiology of IRI during the early reperfusion stage. Oxidative stress can influence the permeability of the inner blood-retina barrier (iBRB), allowing leukocytes access to retinal tissues[37]. The infiltration and activation of immune cells are recognized as the underlying cause of many retinal diseases including ischemic ophthalmia [37, 38]. In UPOAO model, the increase of $CD45^+$ leukocytes and $Iba1^+$ microglia in retina after 3-day reperfusion periods confirmed this viewpoint.

In the later stage of reperfusion (7 days), the DEGs are mainly enriched in immune regulation

and inflammation. With more upregulated DEGs than downregulated ones, we believe that the activation of immune inflammatory response contributes to further IRI in retinal tissue. Previous studies found that the retina can elicit immunological responses during ischemia-reperfusion injury and immune inflammation is an important phenomenon in the progression of this injury [25]. The excessive ROS generated by mitochondria in RGCs during the activation of inflammatory responses can damage cell structure and visual function [39]. Microglia, which are considered as primary resident immune cells, contribute to the inflammatory responses and consequent neural damage [40]. Infiltrating leukocytes can activate resident microglia, forming a feedback loop that exacerbates inflammation [41]. The complex interactions between immune cells and retina neurons after RIRI have been reported [42]. Interestingly, in our result of UPOAO model, the death of major retinal neural cells like RGCs, BCs, HCs correlate with the phase of increased infiltrating leukocytes and resident microglia. Therefore, we considered that the immune response and neuroinflammatory observed after 7 days of reperfusion may be the cumulative effect of the acute oxidative stress and resident and peripheral immune cells responses (**Fig 9**). In a word, we described the pathological processes at different time points and highlight the important role of resident and peripheral Immune cells responses in the UPOAO model. This offers valuable insights for subsequent screening of pathogenic genes and potential immunotherapy approaches.

Compared with HIOP and UCCAO models, the UPOAO model stands out as a more appropriate choice for studying retinal IRI in RAO. The HIOP model, widely used for investigating the pathogenesis of APACG, exhibits retinal degeneration features similar to

the UPOAO model during two reperfusion periods [43]. In our UPOAO model, histologic and immunohistochemical analysis demonstrates that 60 minutes of ischemia followed by 3 days or 7 days reperfusion can cause irreversible damage to the retinal structure and visual function specifically, we observed distinct alterations such as the thinning of the inner retina, substantial apoptosis of RGCs, decreased b-wave. Multiple studies on the HIOP model reported consistent results [40, 44, 45]. However, some typical phenotypes in HIOP model such as thinning of the outer nuclear layer and the entire neuroretina and decreased a-wave were not observed in UPOAO model. moreover, our transcriptome sequence revealed a specific subset of DEGs unique to the UPOAO model, including Apoe, Abca1, Ldlr, Cyp39a1, Bmp6 etc. Notably, these DEGs are significantly enriched in pathways associated with lipid and steroid synthesis. Steroids and lipid metabolism homeostasis is disrupted under conditions of oxidative stress and inflammation [46]. In the UPOAO model, these lipid and steroid biological processes may result from the cumulative pathological responses triggered by IRI, setting it apart from the HIOP model. In the UCCAO model, RNA-seq results showed that DEGs were mainly enriched in two pathways: 1) epigenetic modification-related pathways, including nucleobase-containing compound catabolic process, RNA catabolic process, mRNA catabolic process and N6-methyladenosine (m^6A) modification; 2) cell death pathways, including regulation of autophagosome assembly, negative regulation of neuron death, negative regulation of neuron apoptotic process. Epigenetic mechanisms may play a key role in the pathophysiology of ocular disease [47]. m^6A, one of the most common RNA modifications, has been reported to regulate the cell death processes including apoptosis and autophagy

in the pathological process of IRI [48]. The result suggests that epigenetic mechanisms may significantly influence cell death during UCCAO reperfusion for 7 days. Lee et al. evaluated the characteristics of UCCAO without reperfusion using visual, histologic and immunohistochemical approaches and their results showed delayed perfusion of the ipsilateral retina, thinning of the inner retinal layer 10 weeks after surgery, and dramatic decrease in the amplitudes of b-waves on day 14 after UCCAO [15, 49]. This suggested that UCCAO primarily represents a model of retinal hypoperfusion injury and may not effectively reflect acute ischemic-induced structural and functional damage in RAO (**Fig 9**). The results have led us to consider UPOAO model as an effective experimental model to study pathological processes underlying acute ischemia and IRI.

Our research has certain limitations that should be acknowledged. Firstly, our study focused on the changes occurred within 60 minutes of ischemia and the first 7 days of reperfusion in the UPOAO model. Further exploration is needed to understand changes brought by longer reperfusion time. Additionally, we proposed the possible pathological mechanisms, including iBRB damage, oxidative stress and immune inflammation mainly based on the enrichment results of DEGs at three reperfusion time points. More molecular experimental validation is needed.

In summary, by thoroughly exploring the injury to major retinal neural cells, visual impairment and pathophysiological changes in the UPOAO model, we confirmed that the this model can effectively simulate the acute ischemia-reperfusion processes in RAO and

serve as an ideal mouse model for investigating the underlying ischemia and reperfusion pathological processes. Furthermore, our UPOAO model holds great promise as a novel model for studies of pathogenic genes and potential therapeutic interventions for RAO.

Acknowledgements

The authors would like to express their gratitude to all participants involved in the experiments. The authors also wish to acknowledge the Eye Institute of Renmin Hospital of Wuhan University for providing us with the experimental facilities and environment. Special thanks are extended to Renmin Hospital of Wuhan University for their technical support in certain aspects of the experiments.

Availability of data and materials

All data are available from the corresponding author upon reasonable request.

Authors' contributions

Xiao X and Yang AH conceived the project and supervised, guided the research. Li Y, Wang YD and Feng JQ wrote the draft, Feng JQ, Wang CS, Xie H and Li ZY revised the manuscript. Wang YD and Li Y constructed the animal models and obtained the data. Wang YD and Li Y performed the immunofluorescence staining, HE staining and ERG and data analysis. Li Y and Feng JQ analyzed RNA-seq data and visualization. Wan YW and Wang YD performed the FFA and OCT imaging and Wan YW analyzed the data. Lv BY and Wang YD took pictures and videos of the UPOAO model, and Feng JQ made

schematic diagrams of modeling. Li YM, Xie H, Chen T, Wang FX provided support for the technical methods and contributed to the discussion, and reviewed the manuscript. All authors critically contributed to the manuscript, and have read and approved the final manuscript.

Funding

This work was supported by the National Nature Science Foundation of China (grant number: 82371079), National Key R&D Program of China (2023YFC2308404), Fundamental Research Funds for the Central Universities (2042023gf0013), Key research and development project of Hubei Province (grant number: 2022BCA009).

Ethics approval and consent to participate

All animal experiments were performed following the ethical guidelines outlined in the ARVO Statement for the Use of Animals in Ophthalmic and Vision Research, with the approval of the Experimental Animal Ethics Committee of Renmin Hospital of Wuhan University (approval number: WDRM-20220305A).

References

1. Scott IU, Campochiaro PA, Newman NJ, Biousse V: **Retinal vascular occlusions**. *Lancet* 2020, **396**(10266):1927-1940.
2. Hayreh SS, Zimmerman MB: **Central retinal artery occlusion: visual outcome**. *Am J*

705 *Ophthalmol* 2005, **140**(3):376-391.

706 3. Vestergaard N, Torp-Pedersen C, Vorum H, Aasbjerg K: Risk of Stroke, Myocardial
707 Infarction, and Death Among Patients With Retinal Artery Occlusion and the Effect of
708 Antithrombotic Treatment. *Transl Vis Sci Technol* 2021, 10(11):2.

709 4. Fallico M, Lotery AJ, Longo A, Avitabile T, Bonfiglio V, Russo A, Murabito P, Palmucci S,
710 Pulvirenti A, Reibaldi M: **Risk of acute stroke in patients with retinal artery occlusion: a**
711 **systematic review and meta-analysis**. *Eye (Lond)* 2020, **34**(4):683-689.

712 5. Chen T, Wang Y, Li X, Feng J, Yang H, Li Y, Feng H, Xiao X: Sex differences in major
713 adverse cardiovascular and cerebrovascular event risk among central retinal artery occlusion
714 patients. *Sci Rep* 2023, 13(1):14930.

715 6. Prasad SS, Kojic L, Wen YH, Chen Z, Xiong W, Jia W, Cynader MS: **Retinal gene**
716 **expression after central retinal artery ligation: effects of ischemia and reperfusion**. *Invest*
717 *Ophthalmol Vis Sci* 2010, **51**(12):6207-6219.

718 7. Mac Grory B, Schrag M, Biousse V, Furie KL, Gerhard-Herman M, Lavin PJ, Sobrin L,
719 Tjoumakaris SI, Weyand CM, Yaghi S: **Management of Central Retinal Artery Occlusion: A**
720 **Scientific Statement From the American Heart Association**. *Stroke* 2021, **52**(6):e282-e294.

721 8. Raber FP, Gmeiner FV, Dreyhaupt J, Wolf A, Ludolph AC, Werner JU, Kassubek J,
722 Althaus K: **Thrombolysis in central retinal artery occlusion: a retrospective observational study**.
723 *J Neurol* 2023, **270**(2):891-897.

724 9. Hu H, Zhang B, Zhao Y, Zhou H, Chen H, Yan S: Efficacy of Intra-Arterial Thrombolysis
725 for Acute Central Retinal Artery Occlusion: A Meta-Analysis. *Eur Neurol* 2022, 85(3):186-194.

726 10. Wan P, Su W, Zhang Y, Li Z, Deng C, Li J, Jiang N, Huang S, Long E, Zhuo Y: **LncRNA**

727 **H19 initiates microglial pyroptosis and neuronal death in retinal ischemia/reperfusion injury**.
728 *Cell Death Differ* 2020, **27**(1):176-191.
729 11. Shabanzadeh AP, D'Onofrio PM, Monnier PP, Koeberle PD: **Neurosurgical Modeling of**
730 **Retinal Ischemia-Reperfusion Injury**. *J Stroke Cerebrovasc Dis* 2018, **27**(4):845-856.
731 12. Gao Y, Wu D, Liu D, Huber M, Chen J, Wang X, Lv K, He X, Yang H, Ren C *et al*: **Novel**
732 **Acute Retinal Artery Ischemia and Reperfusion Model in Nonhuman Primates**. *Stroke* 2020,
733 **51**(8):2568-2572.
734 13. Morén H, Undrén P, Gesslein B, Olivecrona GK, Andreasson S, Malmsjö M: **The porcine**
735 **retinal vasculature accessed using an endovascular approach: a new experimental model for**
736 **retinal ischemia**. *Invest Ophthalmol Vis Sci* 2009, **50**(11):5504-5510.
737 14. Zhang Y, Cho CH, Atchaneeyasakul LO, McFarland T, Appukuttan B, Stout JT: **Activation**
738 **of the mitochondrial apoptotic pathway in a rat model of central retinal artery occlusion**. *Invest*
739 *Ophthalmol Vis Sci* 2005, **46**(6):2133-2139.
740 15. Lee D, Kang H, Yoon KY, Chang YY, Song HB: A mouse model of retinal hypoperfusion
741 injury induced by unilateral common carotid artery occlusion. *Exp Eye Res* 2020, 201:108275.
742 16. Lee D, Tomita Y, Miwa Y, Jeong H, Shinojima A, Ban N, Yamaguchi S, Nishioka K,
743 Negishi K, Yoshino J *et al*: **Nicotinamide Mononucleotide Protects against Retinal Dysfunction**
744 **in a Murine Model of Carotid Artery Occlusion**. *Int J Mol Sci* 2022, **23**(23).
745 17. van Zyl T, Yan W, McAdams A, Peng YR, Shekhar K, Regev A, Juric D, Sanes JR: Cell
746 atlas of aqueous humor outflow pathways in eyes of humans and four model species provides
747 insight into glaucoma pathogenesis. *Proc Natl Acad Sci U S A* 2020, 117(19):10339-10349.
748 18. Chen YG, Zhang C, Chiang SK, Wu T, Tso MO: Increased nuclear factor-kappa B p65

749 immunoreactivity following retinal ischemia and reperfusion injury in mice. *J Neurosci Res*
750 2003, 72(1):125-131.
751 19. Ritchie ME, Phipson B, Wu D, Hu Y, Law CW, Shi W, Smyth GK: **limma powers**
752 **differential expression analyses for RNA-sequencing and microarray studies**. *Nucleic Acids*
753 *Res* 2015, **43**(7):e47.
754 20. Subramanian A, Tamayo P, Mootha VK, Mukherjee S, Ebert BL, Gillette MA, Paulovich A,
755 Pomeroy SL, Golub TR, Lander ES *et al*: **Gene set enrichment analysis: a knowledge-based**
756 **approach for interpreting genome-wide expression profiles**. *Proc Natl Acad Sci U S A* 2005,
757 **102**(43):15545-15550.
758 21. Szklarczyk D, Gable AL, Lyon D, Junge A, Wyder S, Huerta-Cepas J, Simonovic M,
759 Doncheva NT, Morris JH, Bork P *et al*: STRING v11: protein-protein association networks with
760 increased coverage, supporting functional discovery in genome-wide experimental datasets.
761 *Nucleic Acids Res* 2019, 47(D1):D607-d613.
762 22. Kohl M, Wiese S, Warscheid B: Cytoscape: software for visualization and analysis of
763 biological networks. *Methods Mol Biol* 2011, 696:291-303.
764 23. Yang Y, Liu W, Sun K, Jiang L, Zhu X: **Tmem30a deficiency leads to retinal rod bipolar**
765 **cell degeneration**. *J Neurochem* 2019, **148**(3):400-412.
766 24. Li G, Ma Q, Wang R, Fan Z, Tao Z, Liu P, Zhao H, Luo Y: Diagnostic and
767 Immunosuppressive Potential of Elevated Mir-424 Levels in Circulating Immune Cells of
768 Ischemic Stroke Patients. *Aging Dis* 2018, 9(2):172-181.
769 25. Minhas G, Sharma J, Khan N: Cellular Stress Response and Immune Signaling in Retinal
770 Ischemia-Reperfusion Injury. *Front Immunol* 2016, 7:444.

771 26. Biousse V, Nahab F, Newman NJ: **Management of Acute Retinal Ischemia: Follow the**
772 **Guidelines!** *Ophthalmology* 2018, **125**(10):1597-1607.
773 27. Block F, Schwarz M: The b-wave of the electroretinogram as an index of retinal ischemia.
774 *Gen Pharmacol* 1998, 30(3):281-287.
775 28. Lima LH, Cella W, Brue C, Tsang SH: Unilateral electronegative ERG in a presumed
776 central retinal artery occlusion. *Clin Ophthalmol* 2010, 4:1311-1314.
777 29. Suzuki R, Oka T, Tamada Y, Shearer TR, Azuma M: Degeneration and dysfunction of
778 retinal neurons in acute ocular hypertensive rats: involvement of calpains. *J Ocul Pharmacol*
779 *Ther* 2014, 30(5):419-428.
780 30. Shinoda K, Yamada K, Matsumoto CS, Kimoto K, Nakatsuka K: Changes in retinal
781 thickness are correlated with alterations of electroretinogram in eyes with central retinal artery
782 occlusion. *Graefes Arch Clin Exp Ophthalmol* 2008, 246(7):949-954.
783 31. Szabo ME, Droy-Lefaix MT, Doly M, Carr é C, Braquet P: Ischemia and
784 reperfusion-induced histologic changes in the rat retina. Demonstration of a free
785 radical-mediated mechanism. *Invest Ophthalmol Vis Sci* 1991, 32(5):1471-1478.
786 32. Szabo ME, Droy-Lefaix MT, Doly M, Braquet P: Ischaemia- and reperfusion-induced Na+,
787 K+, Ca2+ and Mg2+ shifts in rat retina: effects of two free radical scavengers, SOD and EGB
788 761. *Exp Eye Res* 1992, 55(1):39-45.
789 33. Johnson-Léger C, Aurrand-Lions M, Imhof BA: The parting of the endothelium: miracle, or
790 simply a junctional affair? *J Cell Sci* 2000, 113 (Pt 6):921-933.
791 34. Springer TA: Traffic signals for lymphocyte recirculation and leukocyte emigration: the
792 multistep paradigm. *Cell* 1994, 76(2):301-314.

793 35. Fang IM, Yang CM, Yang CH: Chitosan oligosaccharides prevented retinal ischemia and
794 reperfusion injury via reduced oxidative stress and inflammation in rats. *Exp Eye Res* 2015,
795 130:38-50.
796 36. Oharazawa H, Igarashi T, Yokota T, Fujii H, Suzuki H, Machide M, Takahashi H, Ohta S,
797 Ohsawa I: Protection of the retina by rapid diffusion of hydrogen: administration of
798 hydrogen-loaded eye drops in retinal ischemia-reperfusion injury. *Invest Ophthalmol Vis Sci*
799 2010, 51(1):487-492.
800 37. Kaur C, Foulds WS, Ling EA: Blood-retinal barrier in hypoxic ischaemic conditions: basic
801 concepts, clinical features and management. *Prog Retin Eye Res* 2008, 27(6):622-647.
802 38. Eltzschig HK, Collard CD: **Vascular ischaemia and reperfusion injury**. *Br Med Bull* 2004,
803 **70**:71-86.
804 39. Sanderson TH, Reynolds CA, Kumar R, Przyklenk K, Hüttemann M: Molecular
805 mechanisms of ischemia-reperfusion injury in brain: pivotal role of the mitochondrial
806 membrane potential in reactive oxygen species generation. *Mol Neurobiol* 2013, 47(1):9-23.
807 40. Abcouwer SF, Shanmugam S, Muthusamy A, Lin CM, Kong D, Hager H, Liu X, Antonetti
808 DA: **Inflammatory resolution and vascular barrier restoration after retinal ischemia reperfusion**
809 **injury**. *J Neuroinflammation* 2021, **18**(1):186.
810 41. Au NPB, Ma CHE: Neuroinflammation, Microglia and Implications for Retinal Ganglion
811 Cell Survival and Axon Regeneration in Traumatic Optic Neuropathy. *Front Immunol* 2022,
812 13:860070.
813 42. Qin Q, Yu N, Gu Y, Ke W, Zhang Q, Liu X, Wang K, Chen M: Inhibiting multiple forms of
814 cell death optimizes ganglion cells survival after retinal ischemia reperfusion injury. *Cell Death*

815 *Dis* 2022, 13(5):507.

816 43. Yao F, Peng J, Zhang E, Ji D, Gao Z, Tang Y, Yao X, Xia X: Pathologically high
817 intraocular pressure disturbs normal iron homeostasis and leads to retinal ganglion cell
818 ferroptosis in glaucoma. *Cell Death Differ* 2023, 30(1):69-81.

819 44. Zeng Z, You M, Fan C, Rong R, Li H, Xia X: Pathologically high intraocular pressure
820 induces mitochondrial dysfunction through Drp1 and leads to retinal ganglion cell PANoptosis
821 in glaucoma. *Redox Biol* 2023, 62:102687.

822 45. Yang J, Yang N, Luo J, Cheng G, Zhang X, He T, Xing Y: Overexpression of S100A4
823 protects retinal ganglion cells against retinal ischemia-reperfusion injury in mice. *Exp Eye Res*
824 2020, 201:108281.

825 46. Lam T, Harmancey R, Vasquez H, Gilbert B, Patel N, Hariharan V, Lee A, Covey M,
826 Taegtmeyer H: **Reversal of intramyocellular lipid accumulation by lipophagy and a**
827 **p62-mediated pathway**. *Cell Death Discov* 2016, **2**:16061.

828 47. He S, Li X, Chan N, Hinton DR: **Review: Epigenetic mechanisms in ocular disease**. *Mol*
829 *Vis* 2013, **19**:665-674.

830 48. Wang J, Li Y, Zhang S: N(6)-methyladenosine modification: A vital role of programmed
831 cell death in myocardial ischemia/reperfusion injury. *Int J Cardiol* 2022, 367:11-19.

832 49. Lee D, Nakai A, Miwa Y, Tomita Y, Serizawa N, Katada Y, Hatanaka Y, Tsubota K,
833 Negishi K, Kurihara T: **Retinal Degeneration in a Murine Model of Retinal Ischemia by**
834 **Unilateral Common Carotid Artery Occlusion**. *Biomed Res Int* 2021, **2021**:7727648.

835

836

Figures and Tables

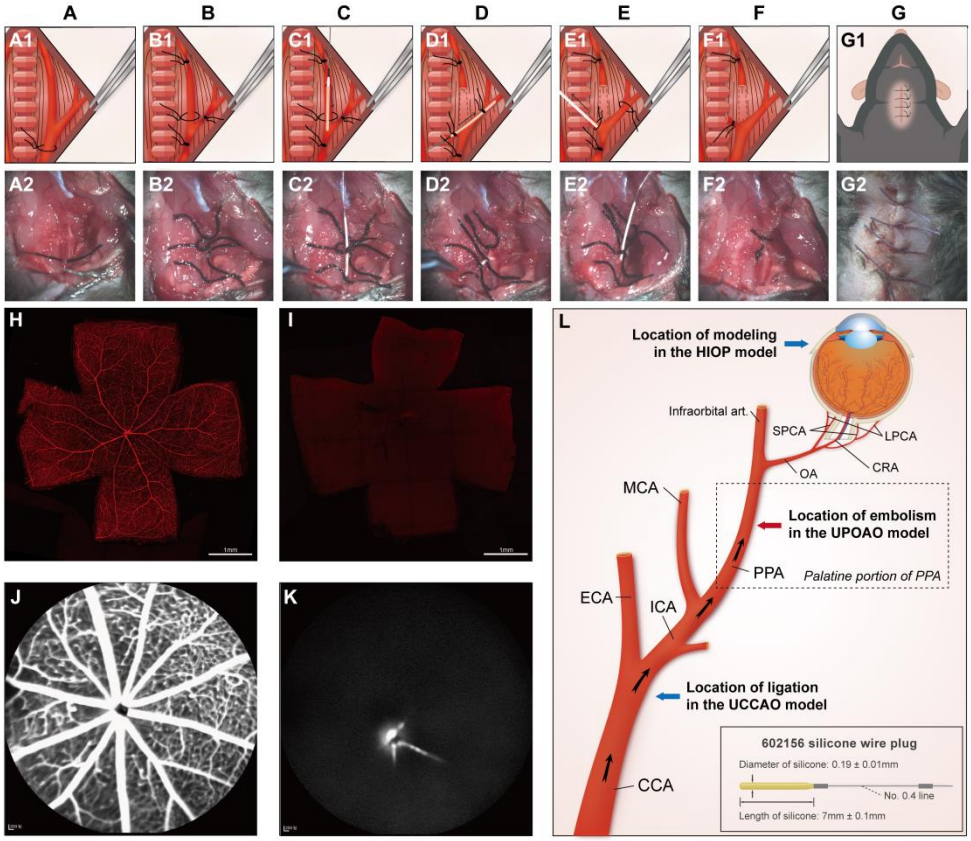

Fig. 1. Modeling Procedure, Validation, and Cervical Artery Anatomy.

(A1-G1) Schematic illustration of unilateral pterygopalatine ophthalmic artery occlusion (UPOAO). (A2-G2) Practical operation of UPOAO. (A1, A2) Blunt separation and left cervical arteries exposure. (B1, B2) Arterial suture ligation. (C1, C2) Silicone wire embolus insertion. The artery was incised a hole and the silicone wire embolus was inserted. (D1, D2) Artery disconnection and movement of the silicone wire embolus. The artery was cut along the hole and the silicone wire embolus was retracted and reinserted. (E1, E2) Removal of the silicone wire embolus and reperfusion. After some time of ischemia, the silicone wire embolus was removed. (F1, F2) Removal of sutures. The sutures at both ends of the disconnected vessel were knotted, and other two sutures were removed. (G1, G2) Anatomic reduction and sutures of the skin. (H and I) Flat-mounted retina after perfusing rhodamine-labeled canavalin A into

the heart of a UPOAO mouse. The sham eye was an unpracticed control eye, and the UPOAO lateral eye was the experimental eye. Retinal vessels in the sham eye (H) were filled with fluorescence while retinal vessels in the UPOAO lateral eye (I) were unfilled. Scale bar = 1 mm. (J and K) Fluorescein Fundus Angiography (FFA) of a UPOAO modeling mouse. The retina vessels (J) were perfused while UPOAO lateral retinal perfusion (K) was delayed. (L) The schematic illustration of cervical artery anatomy and ocular blood supply. Embolization of PPA led to ocular ischemia. The red arrow indicates the embolism site of the silicone wire embolus. The silicone wire embolus is the type 602156 wire embolus extended to 7mm and has a diameter of 0.19mm. The blue arrows indicate the molding locations of the HIOP model and the UCCAO model, respectively. CCA: common carotid artery; ICA: internal carotid artery; ECA: external carotid artery; PPA: pterygopalatine artery; MCA: middle cerebral artery; Post. Sup. Alveolar art.: Posterior superior alveolar artery; Infraorbital art.: infraorbital artery; OA: ophthalmic artery; SPCA: short posterior ciliary artery; LPCA: long posterior ciliary artery; CRA: central retinal artery.

Table 1 Antibodies used in staining of retinal sections

Antibodies	Species	Dilution	Company
PKCα	rabbit	1:1000	Sigma
Recoverin	rabbit	1:1000	Millipore
Calbindin	rabbit	1:5000	SWANT
ChAT	goat	1:200	Millipore
Iba1	rabbit	1:500	Wako

CD45	rabbit	1:100	CST
Rhodamine-labeled canavalin A	/	1:125	MKBio
Goat anti-mouse IgG Alexa Fluor 488	goat	1:500	Jackson
Donkey anti-rabbit IgG Alexa Fluor 594	donkey	1:500	Jackson
Donkey anti-goat IgG Alexa Fluor 488	donkey	1:500	Jackson

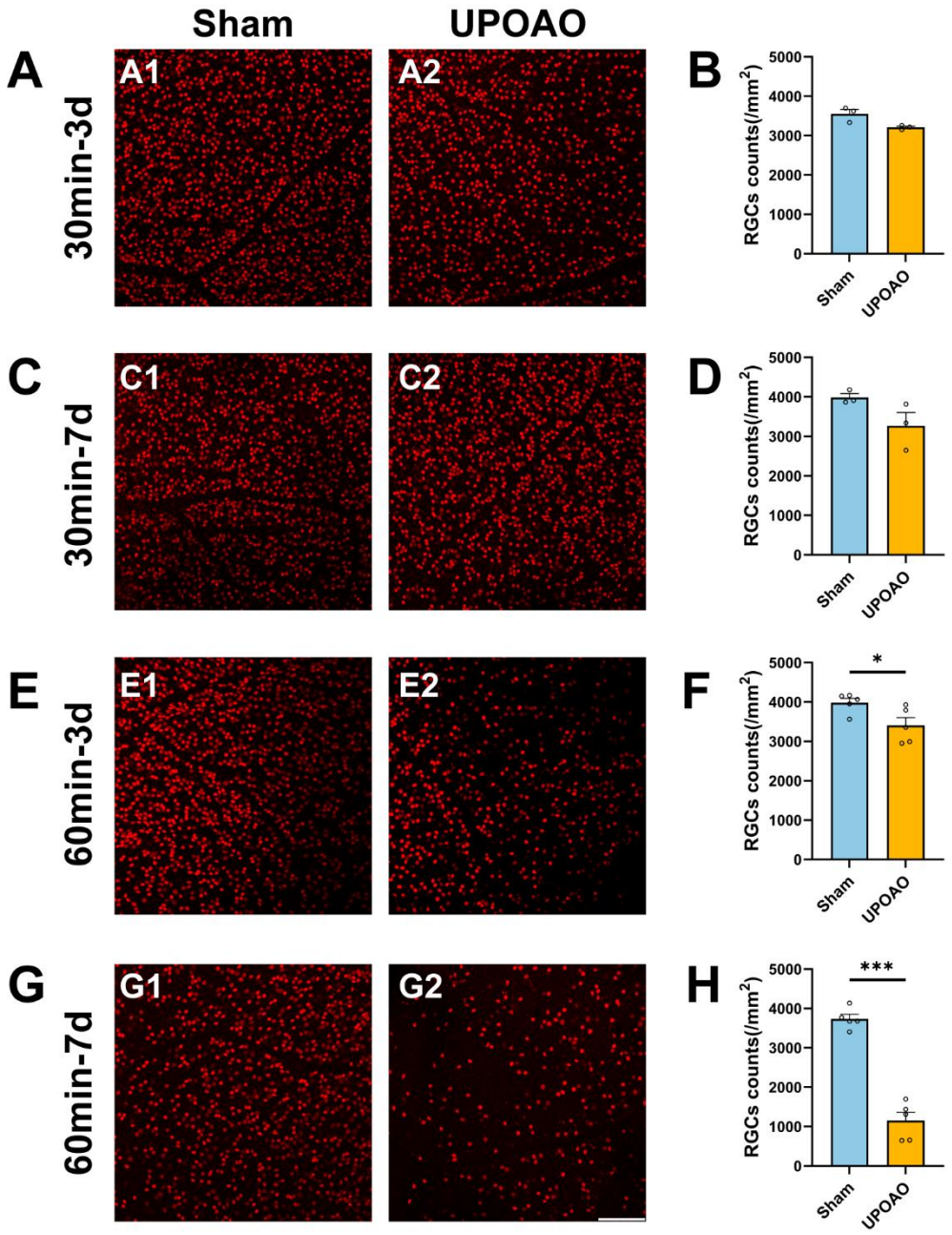

Fig. 2. Staining and quantification of retinal ganglion cells (RGCs) at different ischemia and reperfusion times.

Flat-mounted retina RGCs were labeled with Brn3a staining. (A, B) Representative pictures of peripheral retinal visual field (A), and quantification of surviving RGCs (B) in the 30-minute ischemia and 3-day reperfusion group. N = 3. (C, D) Representative pictures of peripheral retinal visual field (C), and quantification of surviving RGCs (D) in the 30-minute ischemia and

7-day reperfusion group. N = 3. (E, F) Representative pictures of peripheral retinal visual field (E), and quantification of surviving RGCs (F) in the 60-minute ischemia and 3-day reperfusion group. N = 5. (G, H) Representative pictures of peripheral retinal visual field (G), and quantification of surviving RGCs (H) in the 60-minute ischemia and 7-day reperfusion group. N = 5. The results showed the evident RGCs loss after 60-minute ischemia. Data were presented as means ± s.e.m, *: p<0.05, **: p<0.01, ***: p<0.001, ****: p<0.0001, t-test. Scale bar = 100 μm.

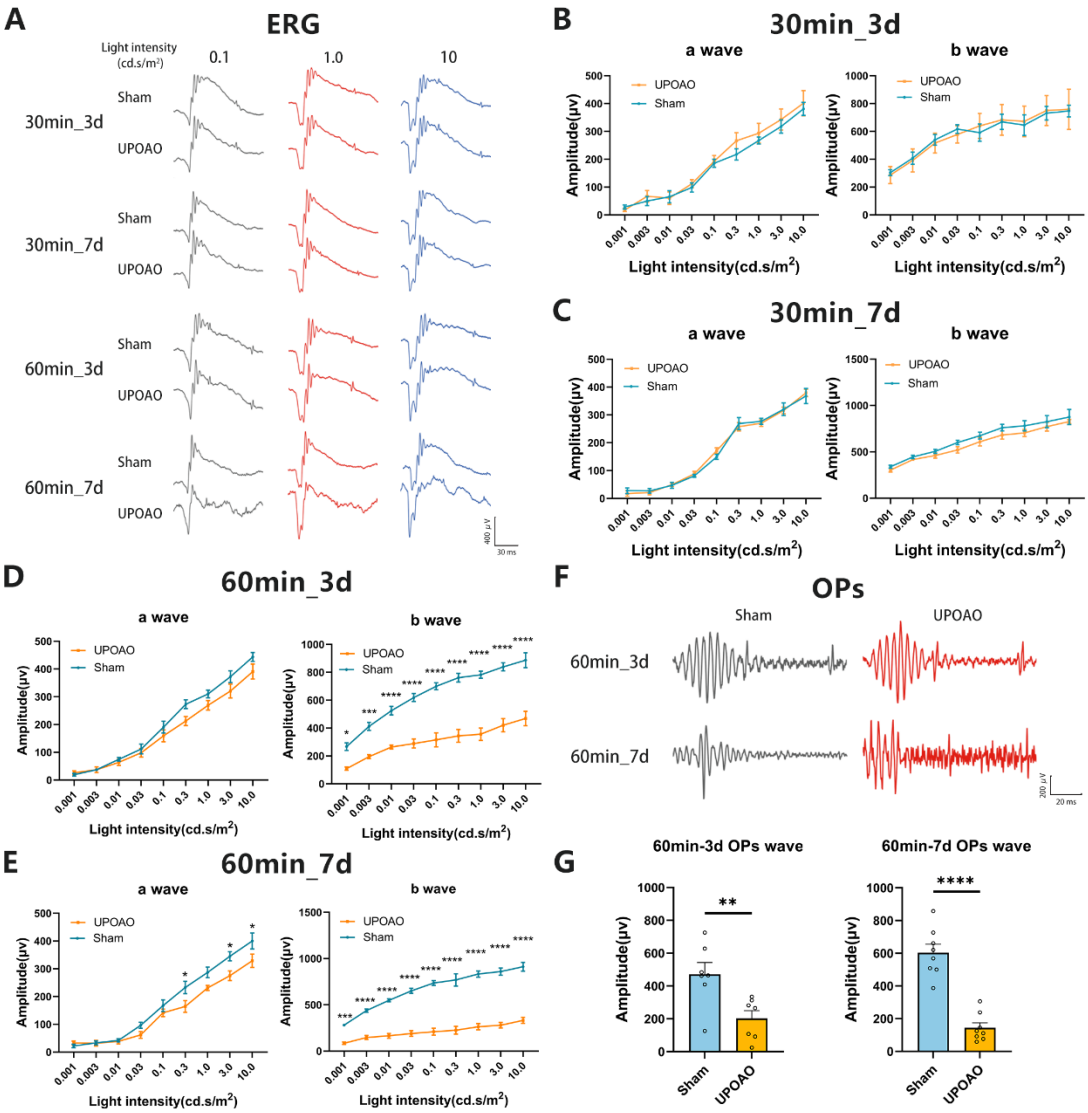

Fig. 3. Comparison of electroretinographic (ERG) dark-adapted responses at different ischemic and reperfusion times.

Following evaluating survival RGCs, visual function between sham vs. UPOAO experimental eyes at different ischemia and reperfusion times was evaluated using ERG. (A) Representative wave lines in four groups at the stimulus light intensity of 0.1, 1.0, and 10.0 cd.s/m2, respectively. (B) Quantification of amplitudes of a-waves and b-waves in the 30-minute ischemia and 3-day reperfusion group. N = 5. (C) Quantification of amplitudes of a-waves and b-waves in the 30-minute ischemia and 7-day reperfusion group. N = 5. (D) Quantification of amplitudes of a-waves, b-waves in the 60-minute ischemia and 3-day reperfusion group. N = 7. (E) Quantification of amplitudes of a-waves and b-waves in the 60-minute ischemia and 7-day reperfusion group. N = 8. Dark-adapted responses were similar in terms of a-wave amplitude but significantly decreased in b-wave amplitude in the 60-minute ischemia groups. The amplitudes of b-waves declined at 3 days and more intensely at 7 days. (F, G) Representative OPs-waves and quantification of amplitudes in the 60-minute ischemic groups. N = 7 in the 3-day reperfusion group; n = 8 in the 7-day reperfusion group. The OPs-wave amplitudes decreased significantly at 7-day reperfusion. The decline of amplitudes in b-waves, OPs-waves, and the loss of RGCs support the selection of a 60-minute ischemic duration as an appropriate choice. Data were presented as means ± s.e.m, *: $p<0.05$, **: $p<0.01$, ***: $p<0.001$, ****: $p<0.0001$, two-way ANOVA test in a-waves and b-waves; paired t-test in OPs-waves.

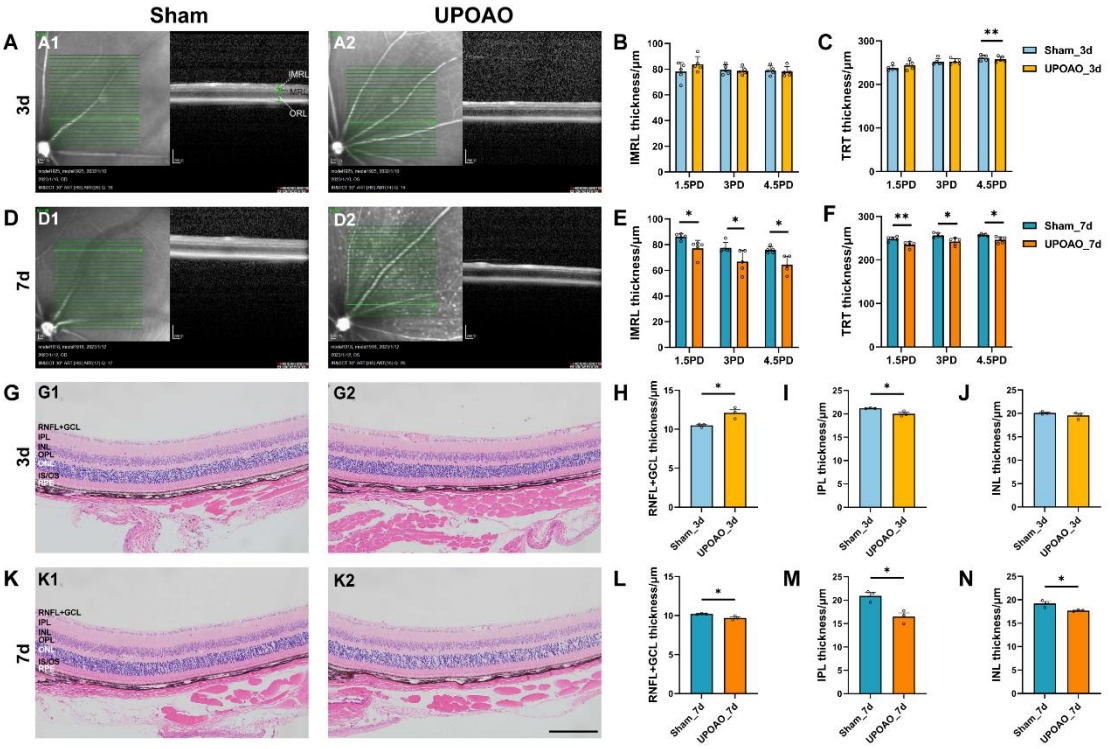

Fig. 4. Changes in retina morphology of the UPOAO animals.

(A) Representative OCT images of mouse retina at 3 days. Green lines indicated the OCT scan area from the optic disc. IMRL: inner middle retina layer, including RNFL, GCL and IPL layers. MRL: middle retina layer, including INL and OPL layers. ORL: outer retina layer, including IS, OS and RPE layers. TRT: total retina thickness, including all layers of the retina. (B and C) Quantification of IMRL and TRT thickness at 3 days. The thickness of IMRL and TRT in OCT was measured and compared at distances of 1.5 PD, 3.0 PD and 4.5 PD from the optic disc, respectively. N = 5. (D) Representative OCT images of mouse retina at 7 days. (E and F) Quantification of IMRL and TRT thickness at 7 days. N = 5. (G) Representative HE images of mouse retina at 3 days. (H, I and J) Quantification of NFL + GCL, IPL and INL thickness at 3 days. Retinal thickness in HE was measured near the optic nerve head and compared. N = 3. (K) Representative HE images of mouse retina at 7 days. (L, M and N) Quantification of NFL + GCL, IPL and INL thickness at 7 days. N = 3. Data were presented as means ± s.e.m, *:

p<0.05, **: p<0.01, ***: p<0.001, ****: p<0.0001, two-way ANOVA test in OCT and paired t-test in HE. PD: papillary diameters; RNFL: retinal nerve fiber layer; GCL: ganglion cell layer; IPL: inner plexiform layer; INL: inner nuclear layer; OPL: outer plexiform layer; IS: inner segment; OS: outer segment; RPE: retinal pigment epithelium. Scale bar = 50 μm.

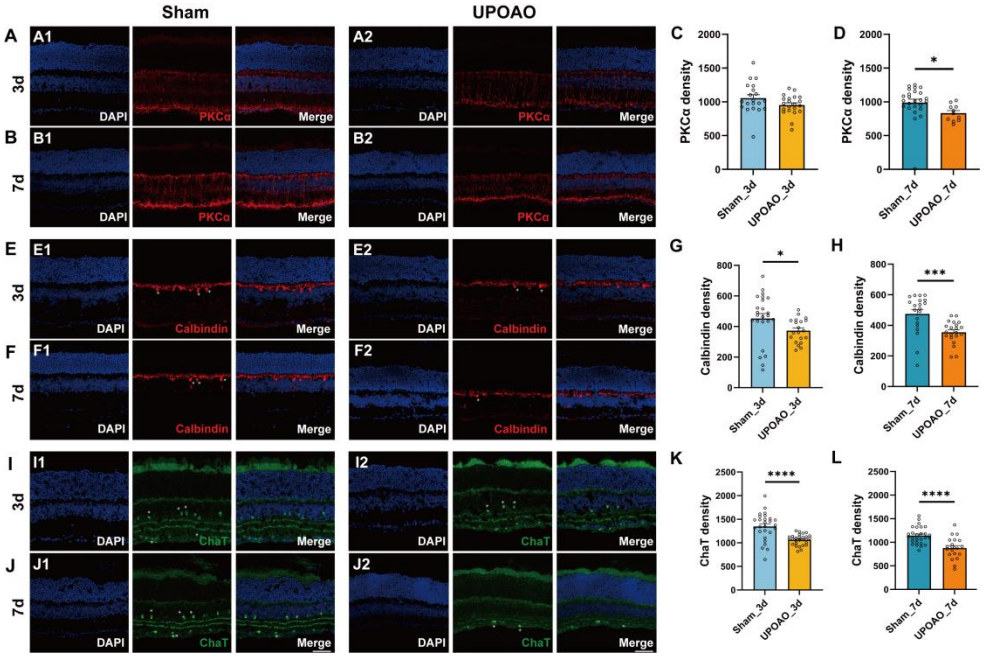

Fig. 5. Changes of bipolar cells, Horizontal cells and cholinergic amacrine cells in the UPOAO mice.

(A) Representative images of DAPI and PKCα co-staining of mouse retina at 3 days. (B) Representative images of DAPI and PKCα co-staining of mouse retina at 7 days. (C) Quantification of PKCα fluorescence density at 3 days. (D) Quantification of PKCα fluorescence density at 7 days. (E) Representative images of DAPI and ChAT co-staining of mouse retina at 3 days. (F) Representative images of DAPI and ChAT co-staining of mouse retina at 7 days. (G) Quantification of ChAT fluorescence density at 3 days. (H) Quantification of ChAT fluorescence density at 7 days. Data points were from sections of four animals. Data

were presented as means ± s.e.m, *: p<0.05, **: p<0.01, ***: p<0.001, ****: p<0.0001, t- test. Scale bar = 50 μm.

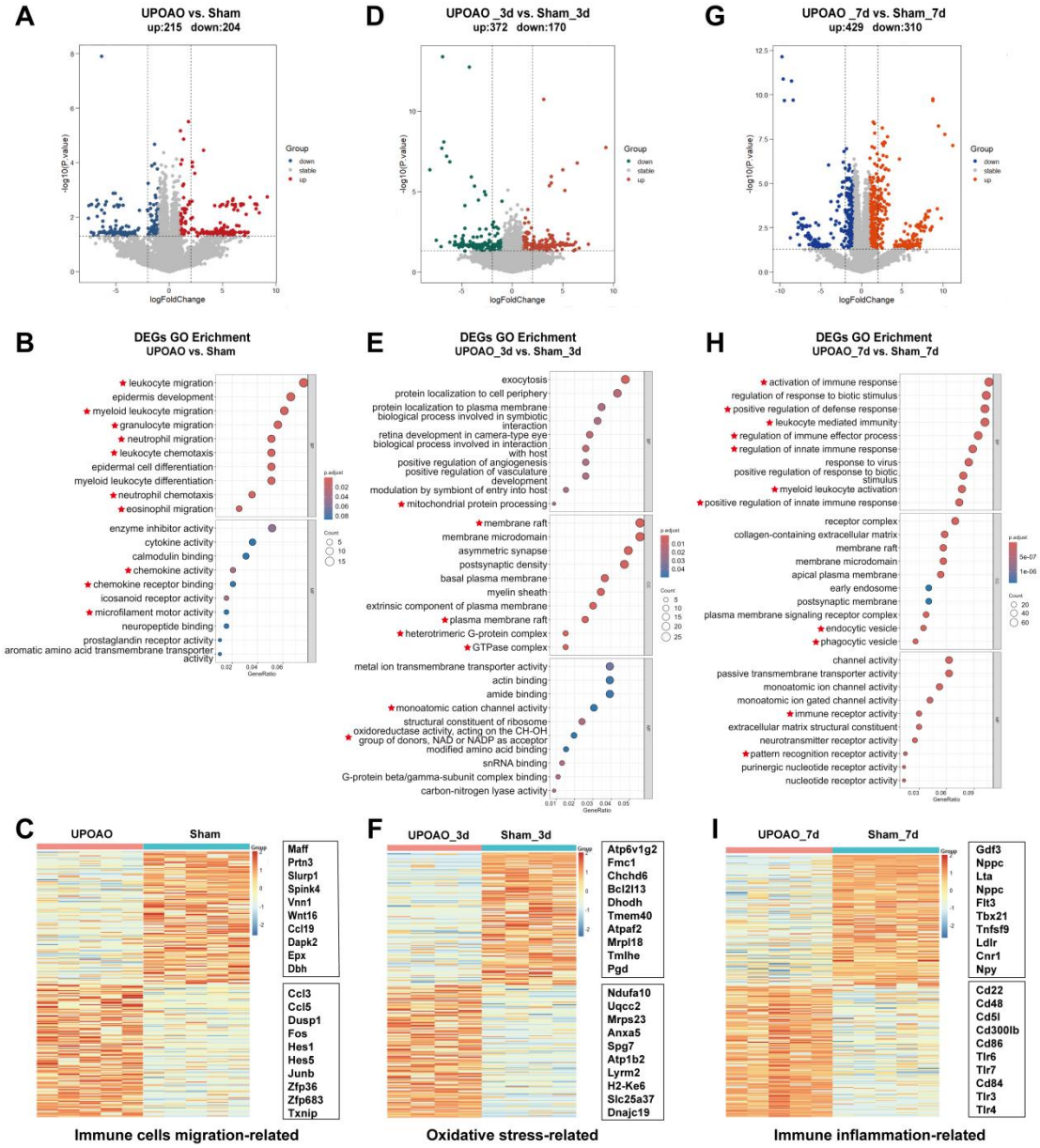

Fig. 6. Transcriptomic features at different times of reperfusion.

RNA-seq evaluation of 0, 3 and 7 days in UPOAO and mostly enriched in the pathways of immune cells migration, oxidative stress and immune inflammation. (A, D, G) Volcano plots showing differential expression genes (DEGs) in the UPOAO and sham eyes in the

no-perfusion group (A), 3-day group (D) and 7-day group (G), respectively. Red dots: significant upregulated genes, green and blue dots: significant downregulated genes, grey dots: stable expressed genes, adjusted $P < 0.05$. log2FC = 1. (B, E, H) Gene ontology (GO) analysis of differential genes in the no-perfusion group (B), 3-day group (E) and 7-day group (H). The overlapping DEGs between UPOAO and Sham eyes were enriched in the pathways of immune cells migration (0d), oxidative stress (3d) and immune inflammation (7d), respectively. (C, F, I) Heatmap showing TOP 150 overlapping DEGs related with pathways of immune cells migration (C), oxidative stress (F) and immune inflammation (I) based on the DEGs between UPOAO and Sham at no-perfusion, 3-day and 7-day reperfusion, respectively. Ranking was determined by the magnitude of fold change. In each heatmap, upper box showed the top 10 up-regulated genes, and the below one showed the top 10 down-regulated genes.

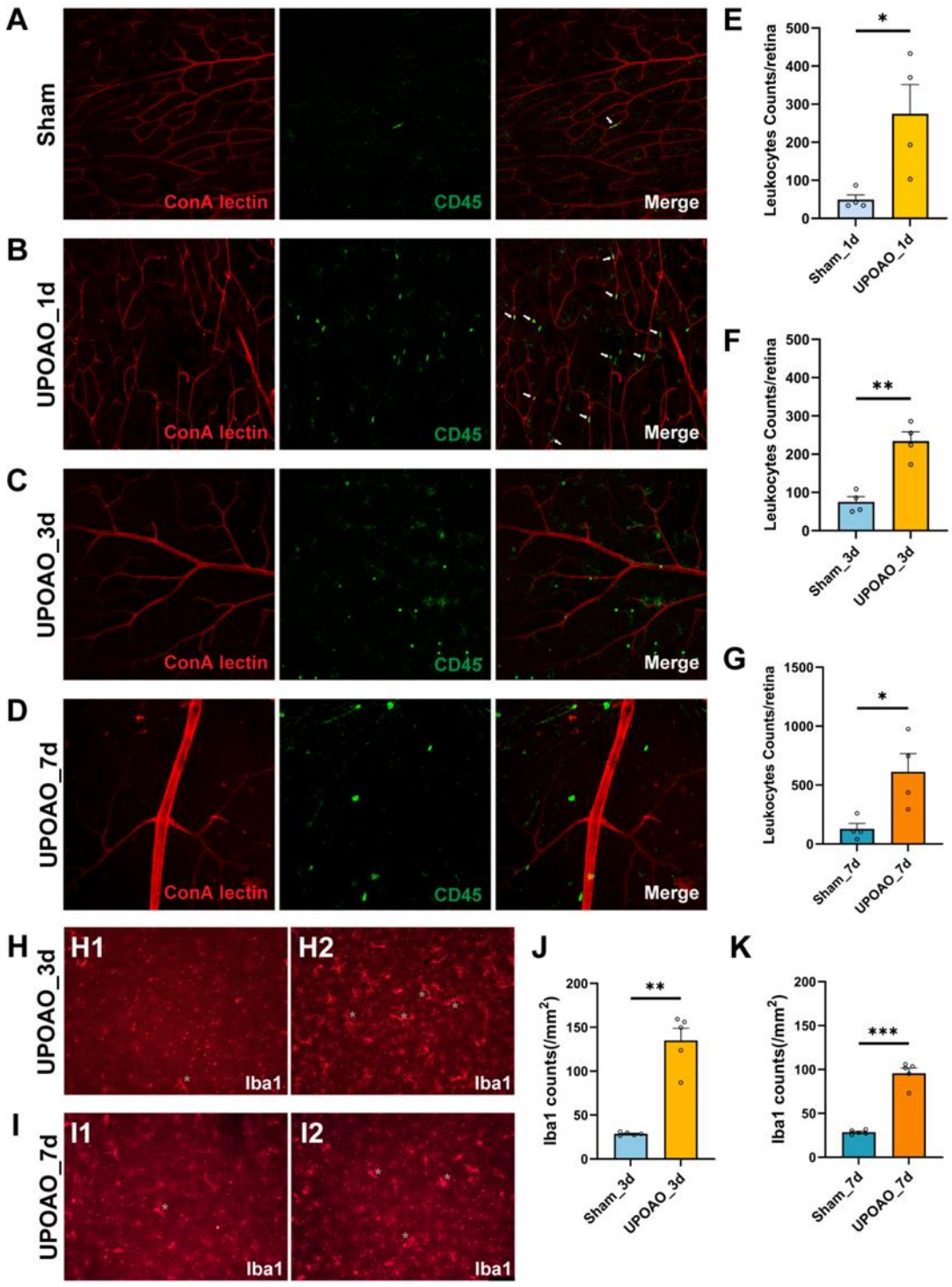

Fig. 7. Peripheral leukocyte infiltration and retinal resident microglial activation. Rhodamine-labeled canavalin A was immediately used for cardiac perfusion to mark blood vessels, followed by CD45 immunofluorescent staining to observe the relationship between blood vessels and $CD45^+$ cells in Sham (A), UPOAO-1d (B), 3d (C), and 7d (D).

The white arrows indicate the presence of $CD45^+$ cells in the blood vessels. UPOAO-1d (E), 3d (F), 7d (G) whole-retinal $CD45^+$ cell counts were performed. The cellular morphology and distribution of microglial cells in the superficial retina of UPOAO-3d (H) and 7d (I). And cell counting of microglial cells in the superficial retina of UPOAO-3d (J) and 7d (K). Data points are from retinal sections of four animals. Data were presented as means ± s.e.m, *: $p<0.05$, **: $p<0.01$, ***: $p<0.001$, ****: $p<0.0001$, t- test. Scale bar = 50 μm.

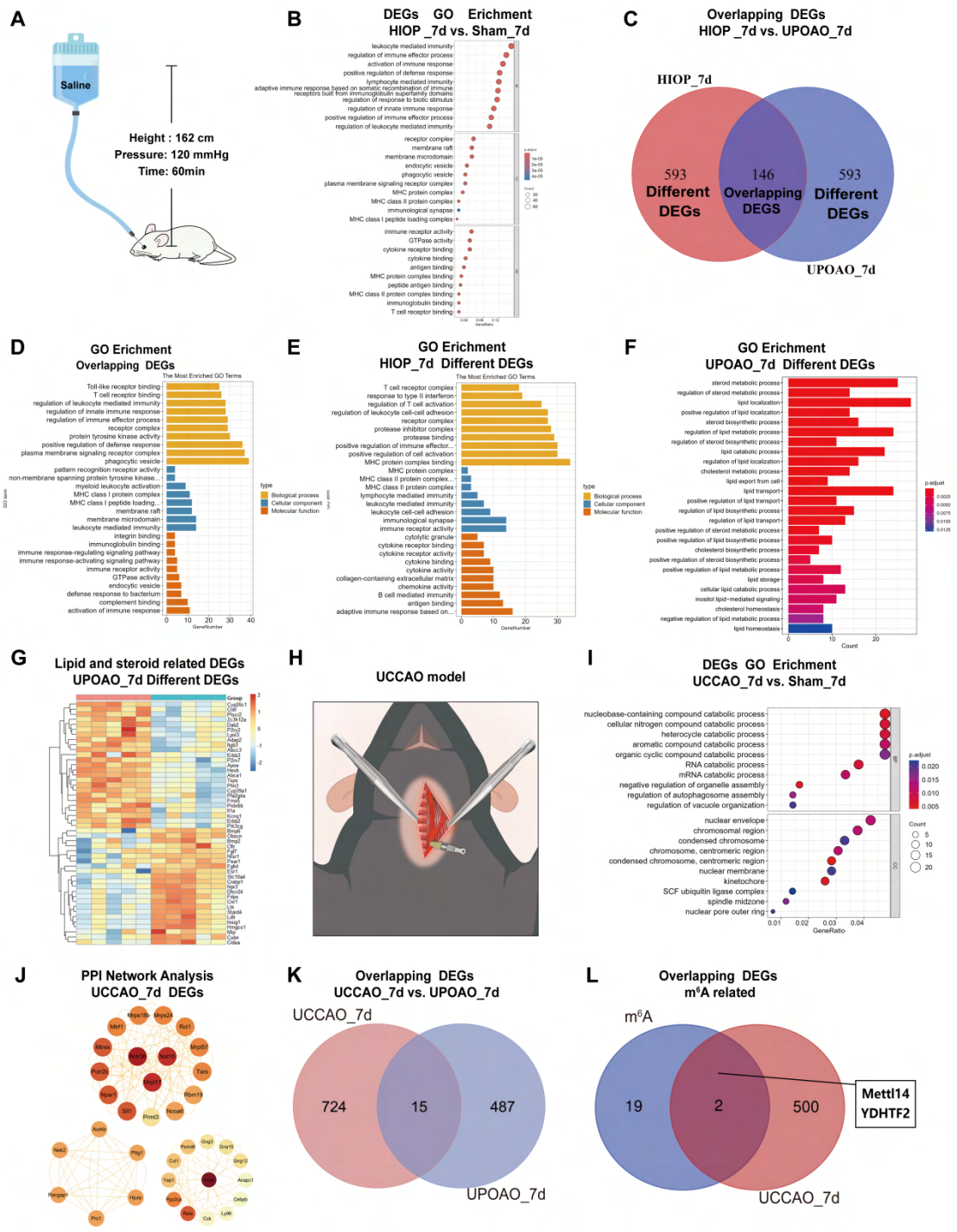

Fig. 8. Transcriptomic results comparison between UPOAO model, HIOP model and UCCAO model.

(A) Schematic illustration of HIOP model. RNA-seq for HIOP retina samples at 7 days. (B) GO analysis of differential genes in the HIOP model. (C) Venn diagram indicating the overlapping DEGs (146 genes) between HIOP and UPOAO and their respective

remaining DEGs (both 593 genes in each group). (D) GO analysis of the overlapping DEGs between HIOP and UPOAO. (E) GO analysis of remaining DEGs in the HIOP_7d model except for overlapping DEGs. (F) GO analysis of remaining DEGs in the UPOAO_7d model. (G) Heatmap showing the inter-sample distribution of lipid and steroid-related DEGs from the analysis of remaining DEGs in the UPOAO model. (H) Schematic illustration of UCCAO model. (I) GO analysis of DEGs in the UCCAO model. (J) Hub genes in PPI network analysis of the DEGs in the UCCAO model were shown. (K) Venn diagram indicating the overlapping DEGs between UCCAO and UPOAO (15 genes). (L) Venn diagram indicated there were two overlapping DEGs between UCCAO DEGs and m6A related genes.

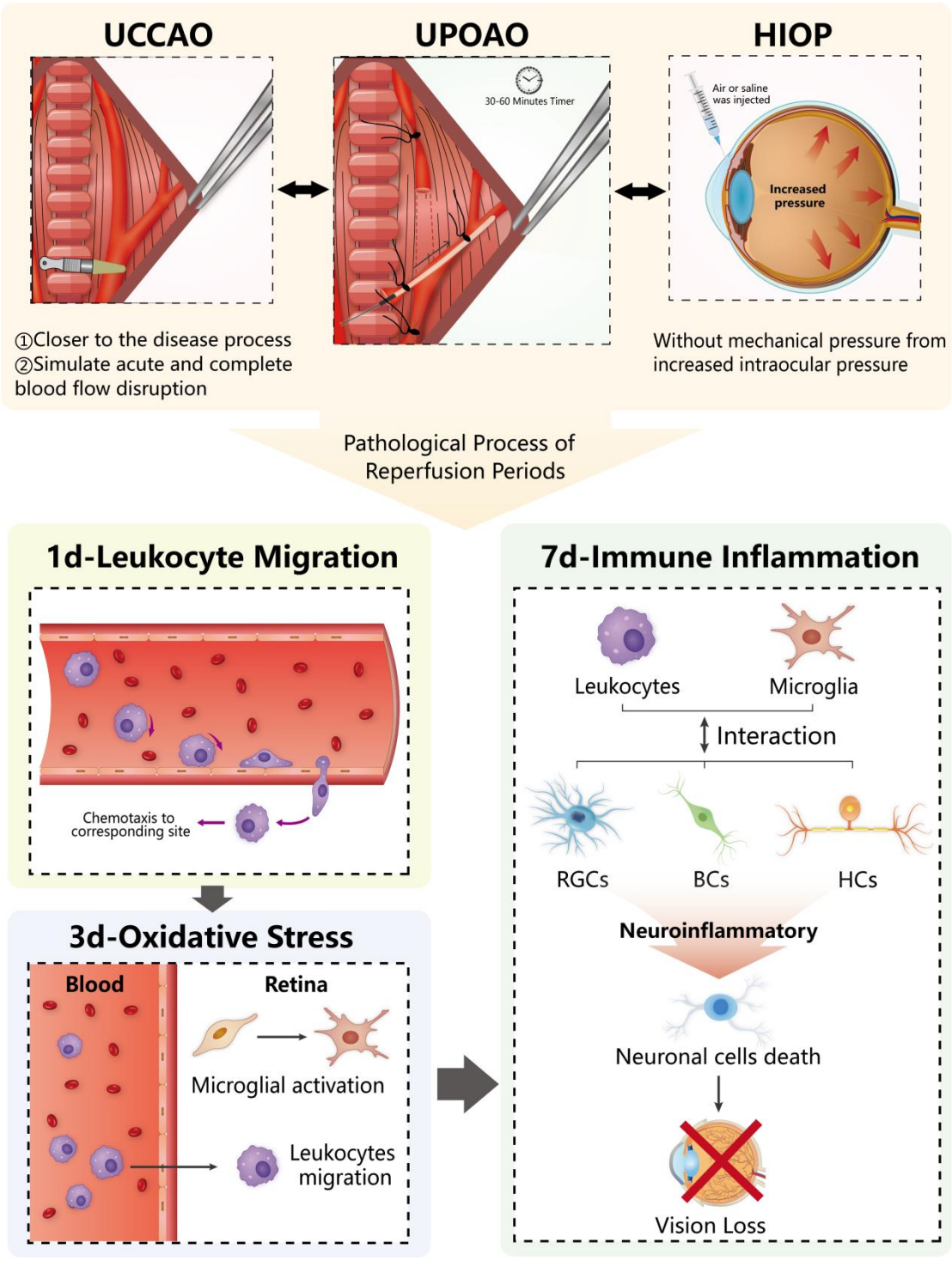

Fig. 9. The characteristic features of UPOAO model in ischemia-reperfusion periods.

Supplementary data

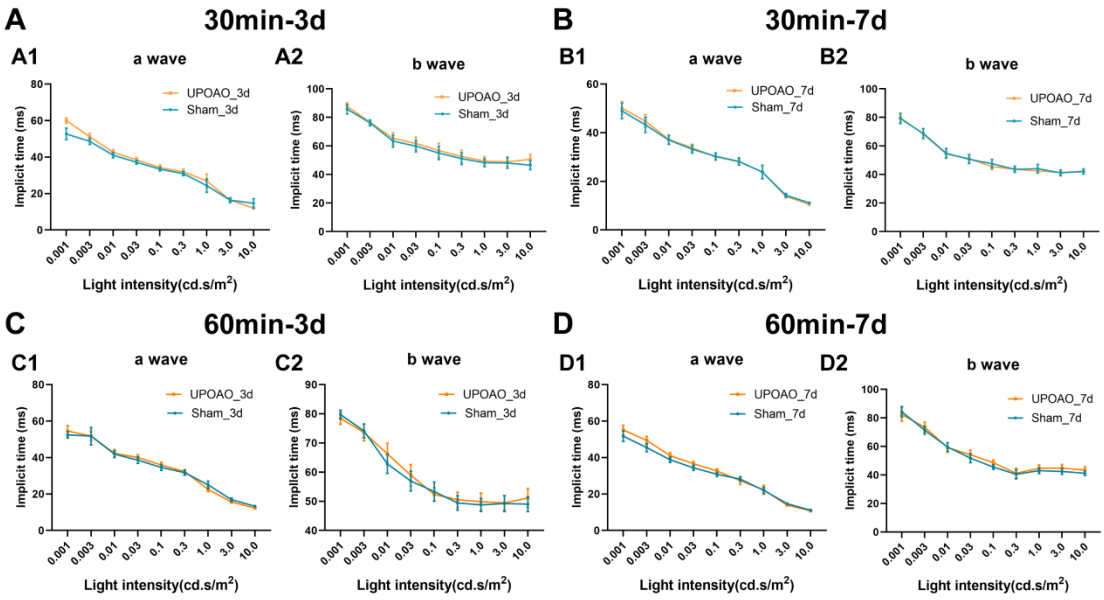

Fig.S1 Response time for a-waves and b-waves in ERG under different light intensities. (A, B) Response times of a-waves and b-waves under different light intensities at 3 and 7 days post-UPOAO in the 30-minute ischemia group. (C, D) Response times of a-waves and b-waves under different light intensities at 3 and 7 days post-UPOAO in the 60-minute ischemia group. Data were presented as means ± s.e.m, *: $p<0.05$, **: $p<0.01$, ***: $p<0.001$, ****: $p<0.0001$, two-way ANOVA test.

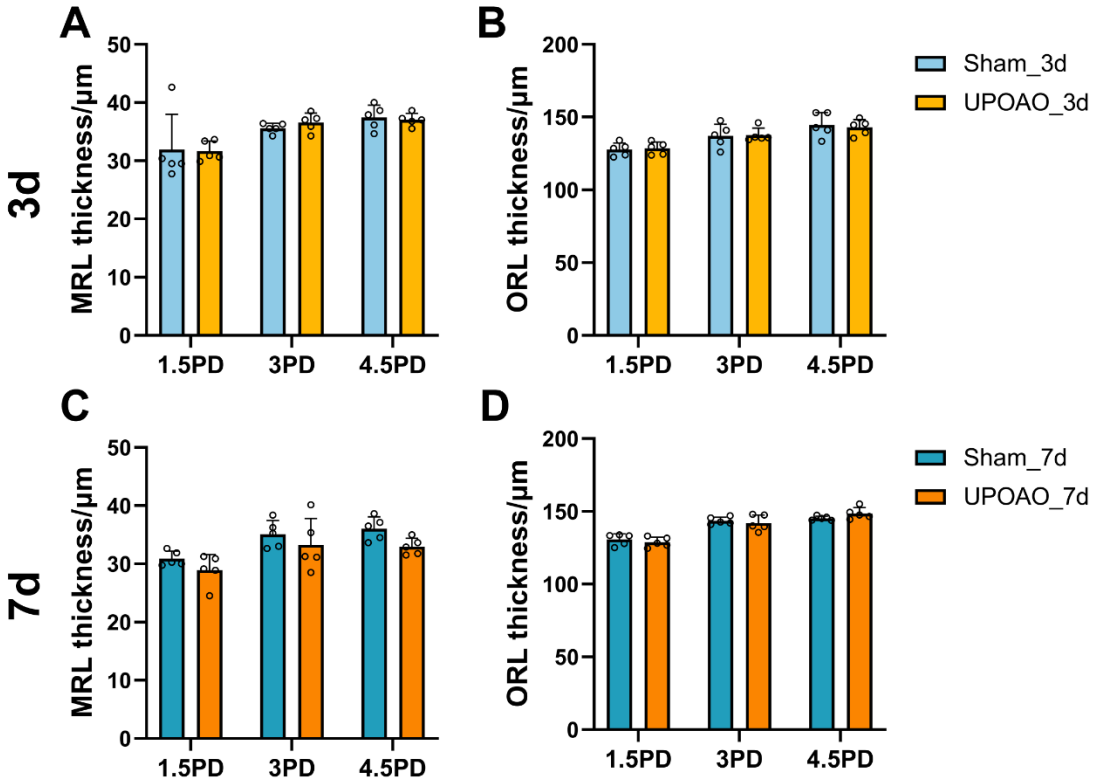

Fig.S1 Quantification of MRL and ORL thickness in OCT at 3-d and 7-d reperfusion of the UPOAO animals.

MRL and ORL thickness in OCT were measured and compared at distances of 1.5 PD, 3.0 PD and 4.5 PD from the optic disc, respectively. (A and B) Quantification of MRL (A) and ORL (B) thickness at 3 days. n = 5. No significant differences. (C and D) Quantification of MRL (C) and ORL (D) thickness at 7 days. N = 5. No significant differences. Data were presented as means ± s.e.m, *: p<0.05, **: p<0.01, ***: p<0.001, ****: p<0.0001, two-way ANOVA test.

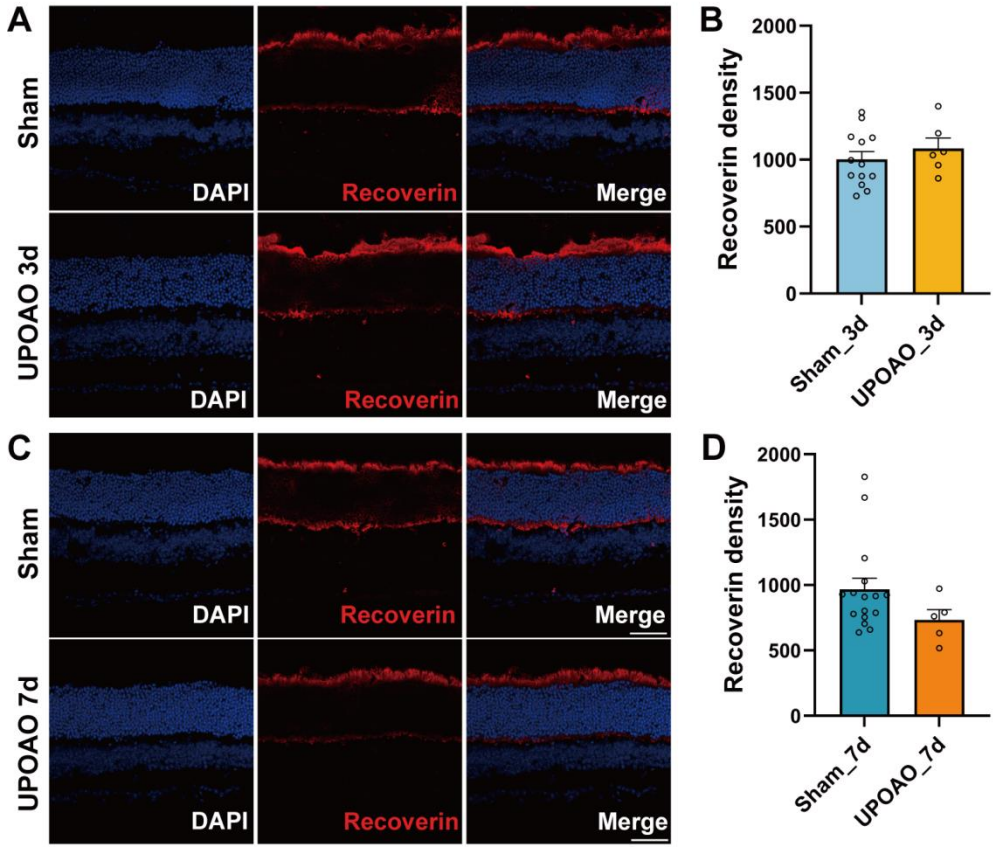

Fig.S2 Changes of photoreceptor cells in the UPOAO mice.

(A) Representative images of DAPI and Recoverin co-staining of mouse retina at 3 days. (B) Representative images of DAPI and Reconerin co-staining of mouse retina at 7 days. Data points were from sections of four animals. Data were presented as means ± s.e.m, *: $p<0.05$, **: $p<0.01$, ***: $p<0.001$, ****: $p<0.0001$, t- test. Scale bar = 50 μm.

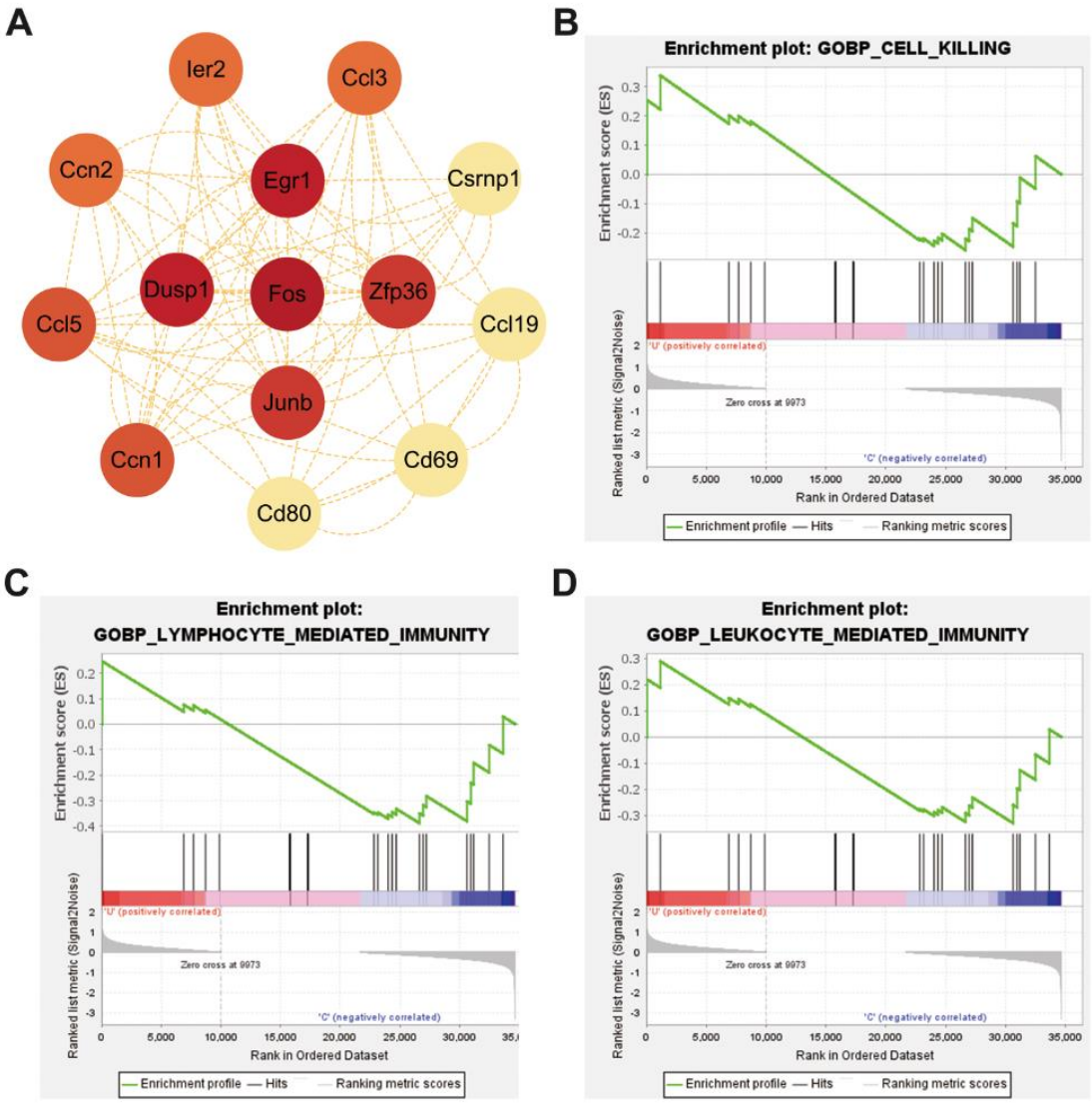

Fig.S4 Hub genes in PPI analysis and GSEA analysis at no-reperfusion in UPOAO.

(A) Hub genes in PPI analysis of DEGs at no-reperfusion group. (B-D) GSEA analysis of the pathway of the cell killing (B), leukocyte mediated-immunity (C) and lymphocyte mediated-immunity (D) at no-reperfusion group.

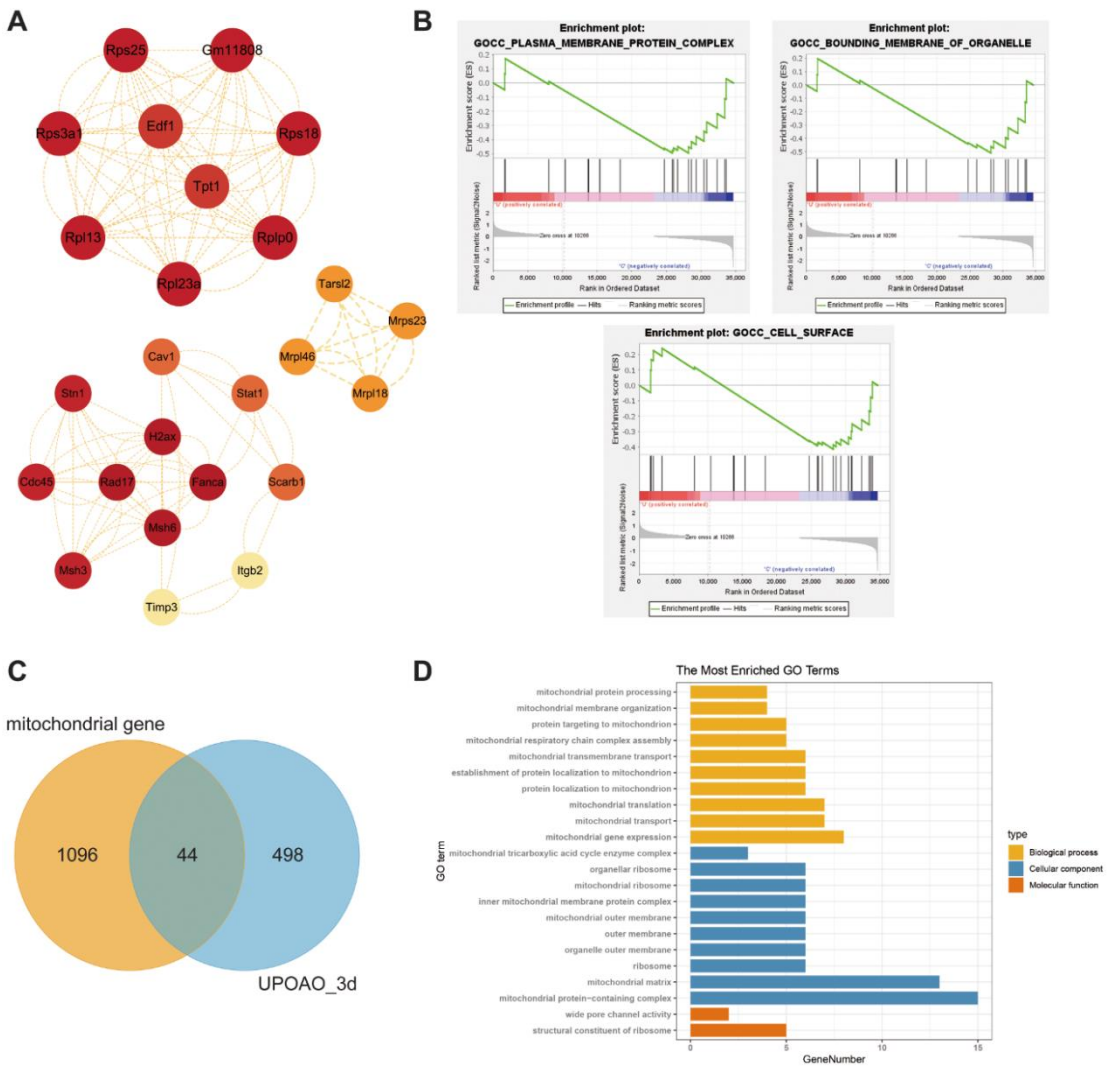

Fig.S5 Hub genes, GSEA analysis at 3-day reperfusion in UPOAO and relation with mitochondrial genes.

(A) Hub genes in PPI analysis of DEGs at 3-day reperfusion group. (B) GSEA analysis of the pathway of plasma membrane protein complex (top left), bounding membrane of organelle (top right) and cell surface (bottom). (C) Venn diagram of mitochondrial genes and DEGs at 3-day reperfusion (44 genes). (D) GO analysis of 44 overlapping DEGs.

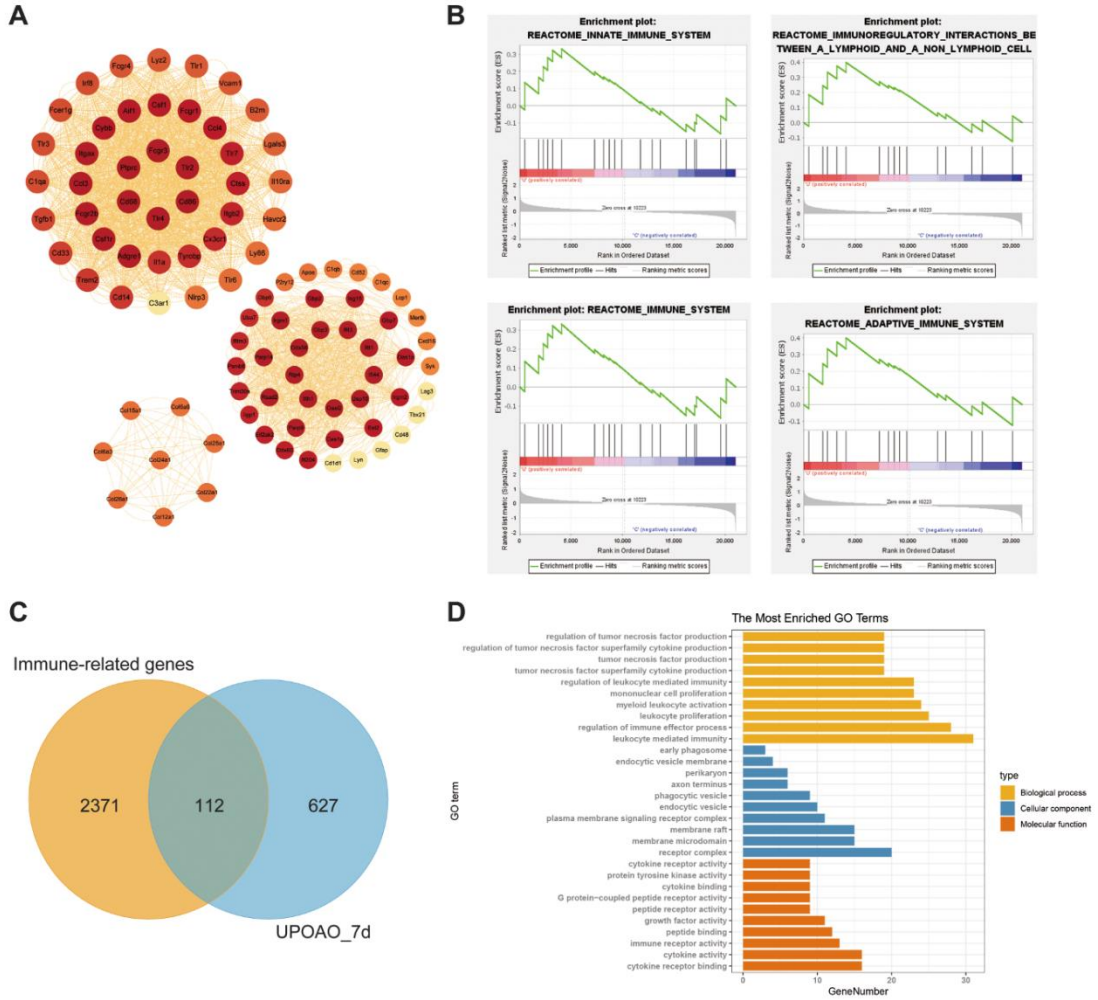

Fig.S6 Hub genes, GSEA analysis at 7-day reperfusion in UPOAO and relation with immune genes.

(A) Hub genes in PPI analysis of DEGs at 7-day reperfusion group. (B) GSEA analysis of the pathway of reactome innate immune system (top left), reactome immunoregulatory interactions between a lymphoid and a non-lymphoid cell (top right), reactome immune system (bottom left) and reactome adaptive immune system (bottom right). (C) Venn diagram of immune genes and DEGs at 7-day reperfusion (112 genes). (D) GO analysis of 112 overlapping DEGs.

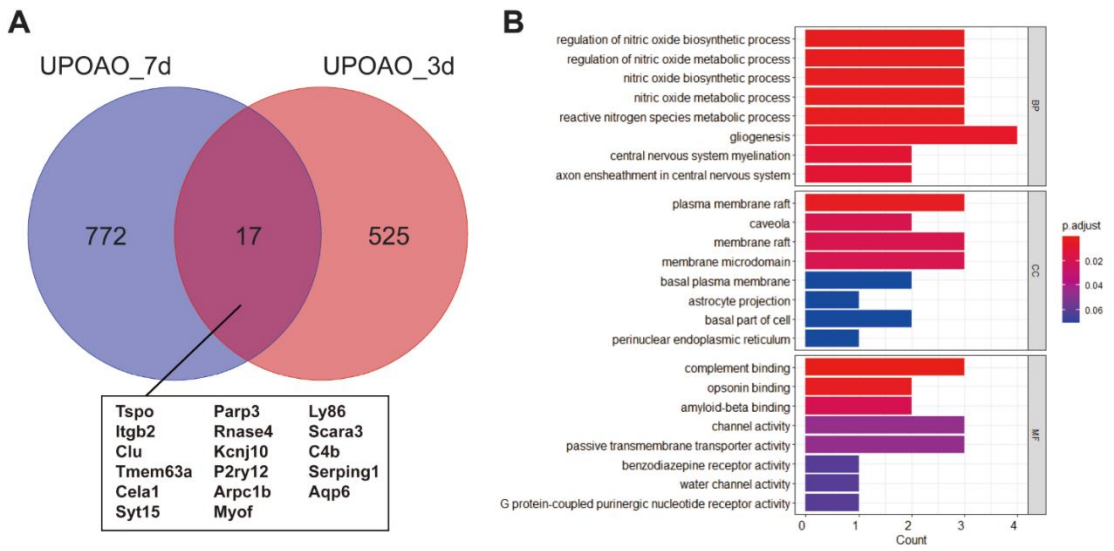

Fig.S7 The co-expressed genes for 3-day and 7-day reperfusion.

(A) Venn diagram of DEGs at 3-day and 7-day reperfusion and list of 17 overlapping DEGs. (B) GO analysis of 17 overlapping DEGs.

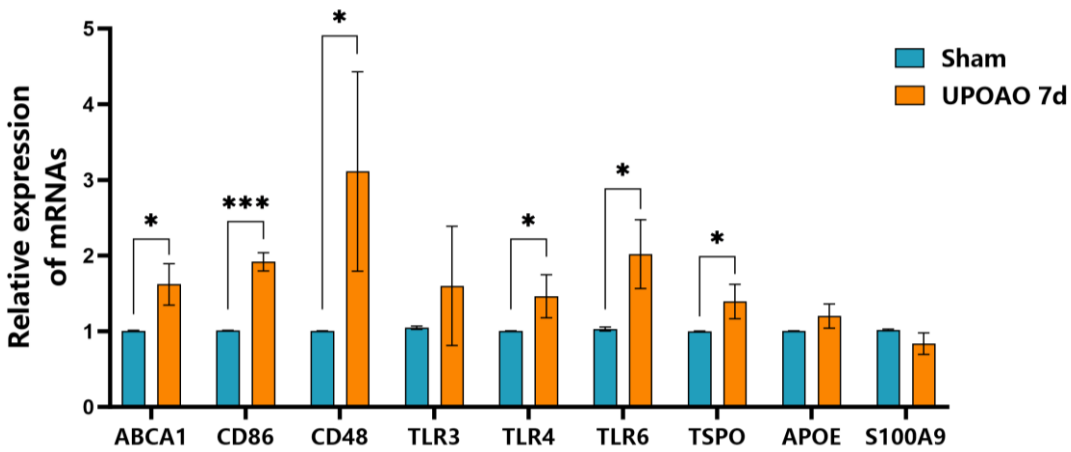

Fig.S8 Immune inflammation-related gene expression was upregulated in the UPOAO-7d group.

ABCA1, CD86, CD48, TLR4, TLR6, and TSPO genes were significantly upregulated in the UPOAO-7d group, while other immune-inflammatory and chemotaxis-related genes showed no significant differences. The data points are from retina of four animals. Data

were presented as means ± s.e.m, *: p<0.05, **: p<0.01, ***: p<0.001, ****: p<0.0001, Paired t-test.

Table. S1 List of primers used in this study.

Gene Name		Sequence (5'->3')
Tlr3	Forward primer	CGATTCCCGACCAGCACTCT
	Reverse primer	CACATTTCCTTTCAGCCTGTGAT
Tlr4	Forward primer	TCCCTGCATAGAGGTAGTTCC
	Reverse primer	TCAAGGGGTTGAAGCTCAGA
Cd48	Forward primer	GGAACTGGATTTCAAGGTCATTCA
	Reverse primer	ATGGTCCAAGTGGGTCCTTAT
Ldlr	Forward primer	CCAATCGACTCACGGGTTCA
	Reverse primer	ACAGTGTCGACTTCTCTAGGC
Cd86	Forward primer	ATGGACCCCAGATGCACCA
	Reverse primer	TGTGCCCAAATAGTGCTCGT
Tspo	Forward primer	ACTGTATTCAGCCATGGGGTATG
	Reverse primer	CCAAGGGAACCATAGCGTCC
Abca1	Forward primer	GCAAGGCCGCACCATTATTT
	Reverse primer	TCTGAGAAACACTGTCCTCCTTTT
Apoe	Forward primer	CGGGTGCTCTGTTTTGGAGA
	Reverse primer	GGCTAGGCATCCTGTCAGC
S100a9	Forward primer	TGGCAACCTTTATGAAGAAAGAGA

	Reverse primer	GTGGGTTGTTCTCATGCAGC
β-actin	Forward primer	CACTGTCGAGTCGCGTCC
	Reverse primer	TCATCCATGGCGAACTGGTG

Video 1. Blunt dissection of cervical vessels. Neck was exposed and cervical arteries were bluntly separated.

Video 2. Insertion of the silicone wire embolus and ischemia. The silicone wire embolus was inserted into the PPA and ischemia began. PPA: the pterygopalatine artery.

Video 3. Extraction of the silicone wire embolus and reperfusion. The silicone wire embolus was removed and reperfusion began. The mouse's wound was sutured, and standard feeding procedures were followed.

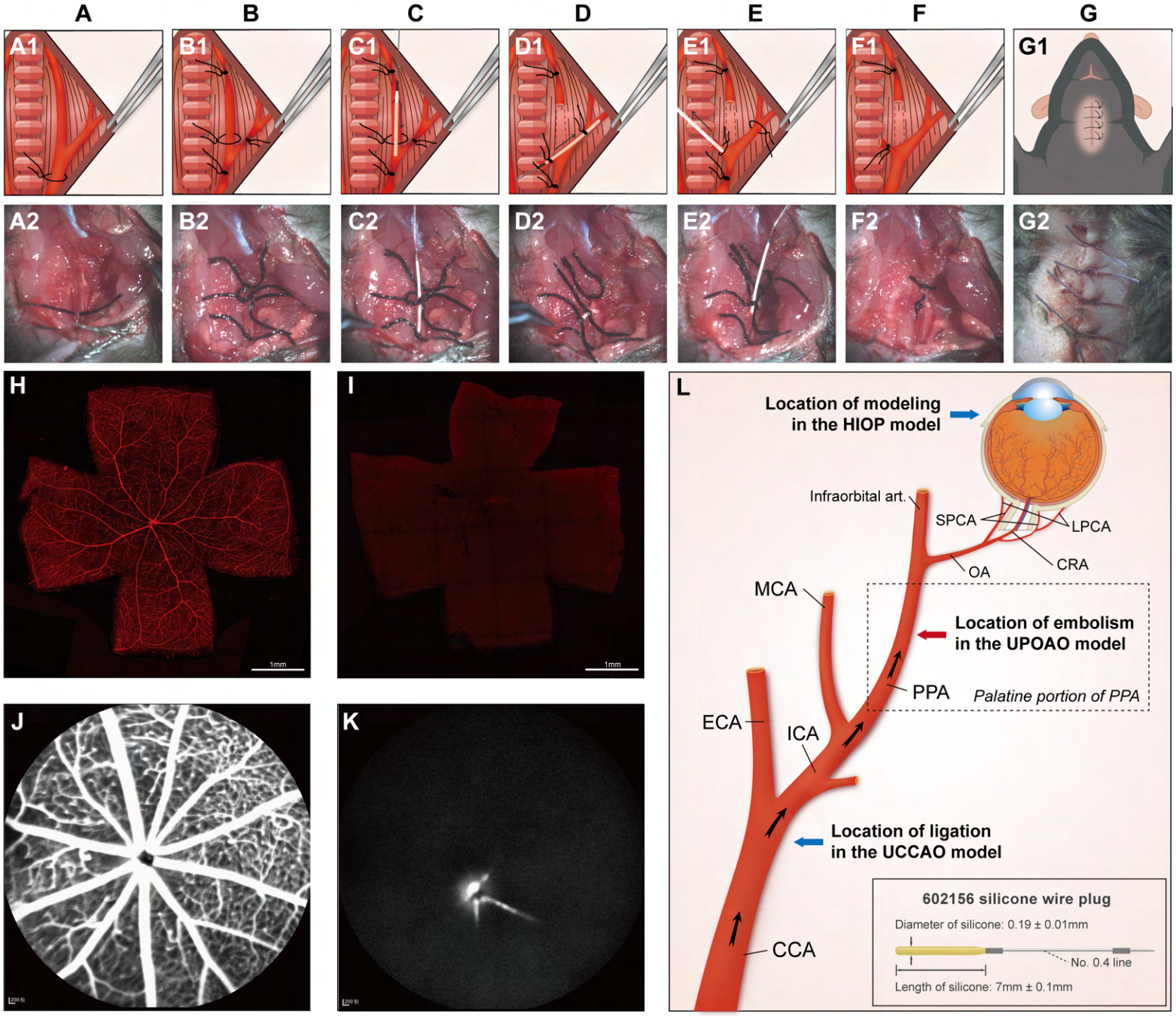
A
B
C
D
E
F
G
A1
B1
C1
D1
E1
F1
G1
A2
B2
C2
D2
E2
F2
G2
H
1mm
I
1mm
J
K
L
Location of modeling in the HIOP model
Infraorbital art.
SPCA
LPCA
CRA
OA
MCA
Location of embolism in the UPOAO model
PPA
Palatine portion of PPA
ECA
ICA
Location of ligation in the UCCAO model
CCA
602156 silicone wire plug
Diameter of silicone: 0.19 ± 0.01mm
No. 0.4 line
Length of silicone: 7mm ± 0.1mm

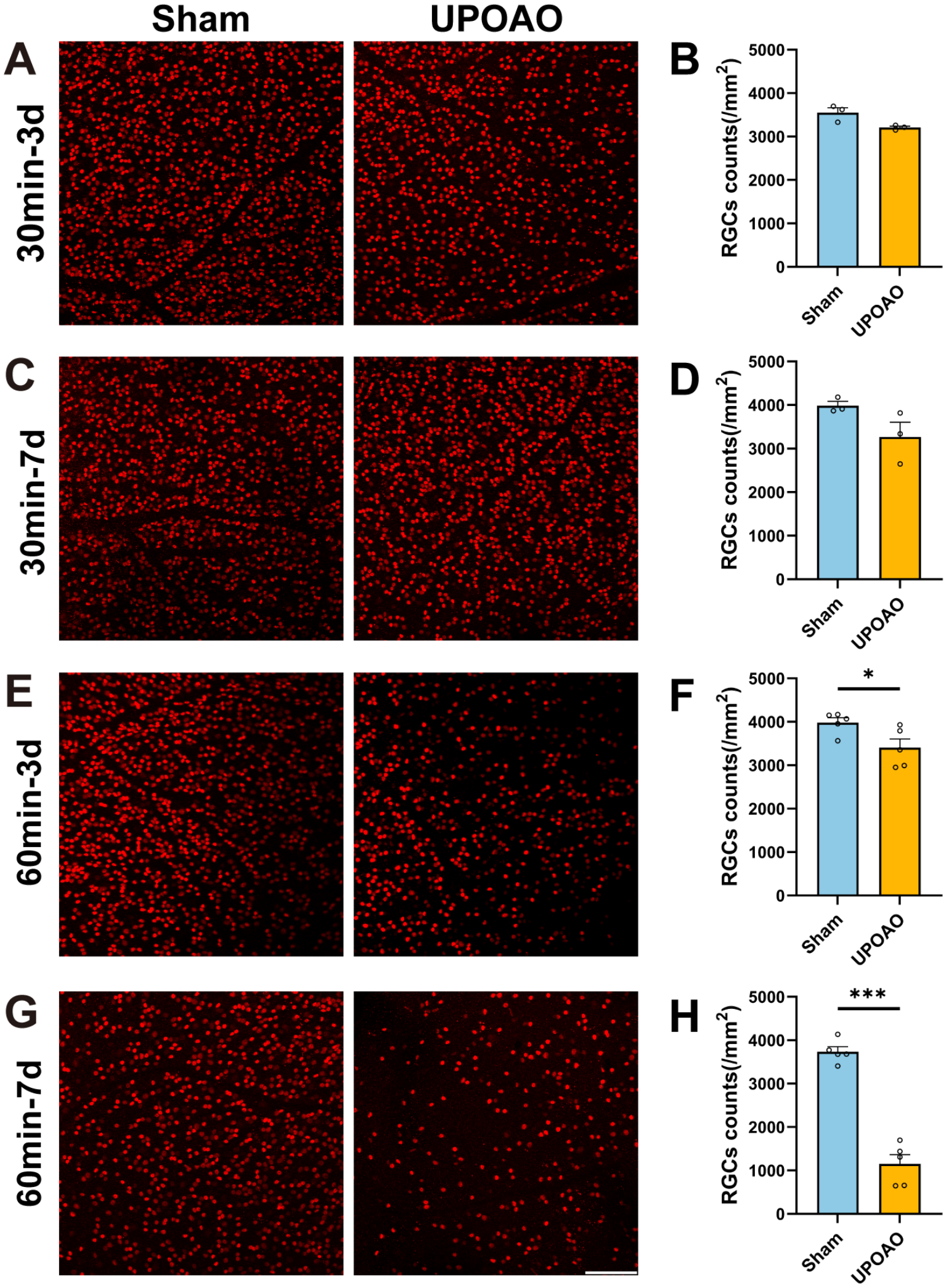
Sham
UPOAO
A
30min-3d
B
RGCs counts(/mm2)
5000
4000
3000
2000
1000
0
Sham
UPOAO
C
30min-7d
D
RGCs counts(/mm2)
5000
4000
3000
2000
1000
0
Sham
UPOAO
E
60min-3d
F
*
RGCs counts(/mm2)
5000
4000
3000
2000
1000
0
Sham
UPOAO
G
60min-7d
H
***
RGCs counts(/mm2)
5000
4000
3000
2000
1000
0
Sham
UPOAO

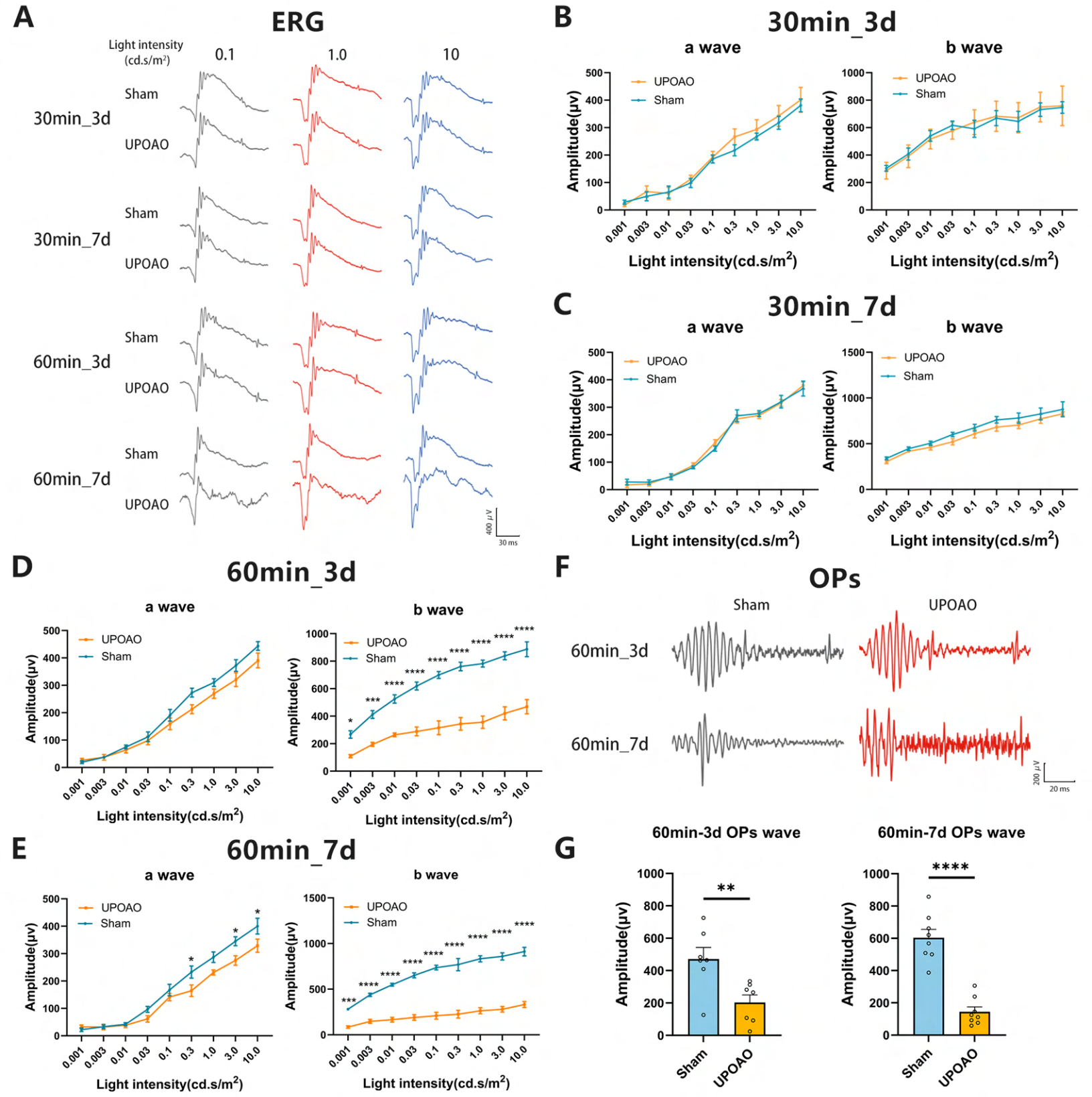
A
ERG
Light intensity (cd.s/m²)
0.1
1.0
10
30min_3d
30min_7d
60min_3d
60min_7d
Sham
UPOAO
400 μV
30 ms
B
30min_3d
a wave
b wave
UPOAO
Sham
Amplitude(μv)
Light intensity(cd.s/m²)
C
30min_7d
D
60min_3d
E
60min_7d
F
OPs
60min_3d
60min_7d
200 μV
20 ms
G
60min-3d OPs wave
60min-7d OPs wave
Sham
UPOAO

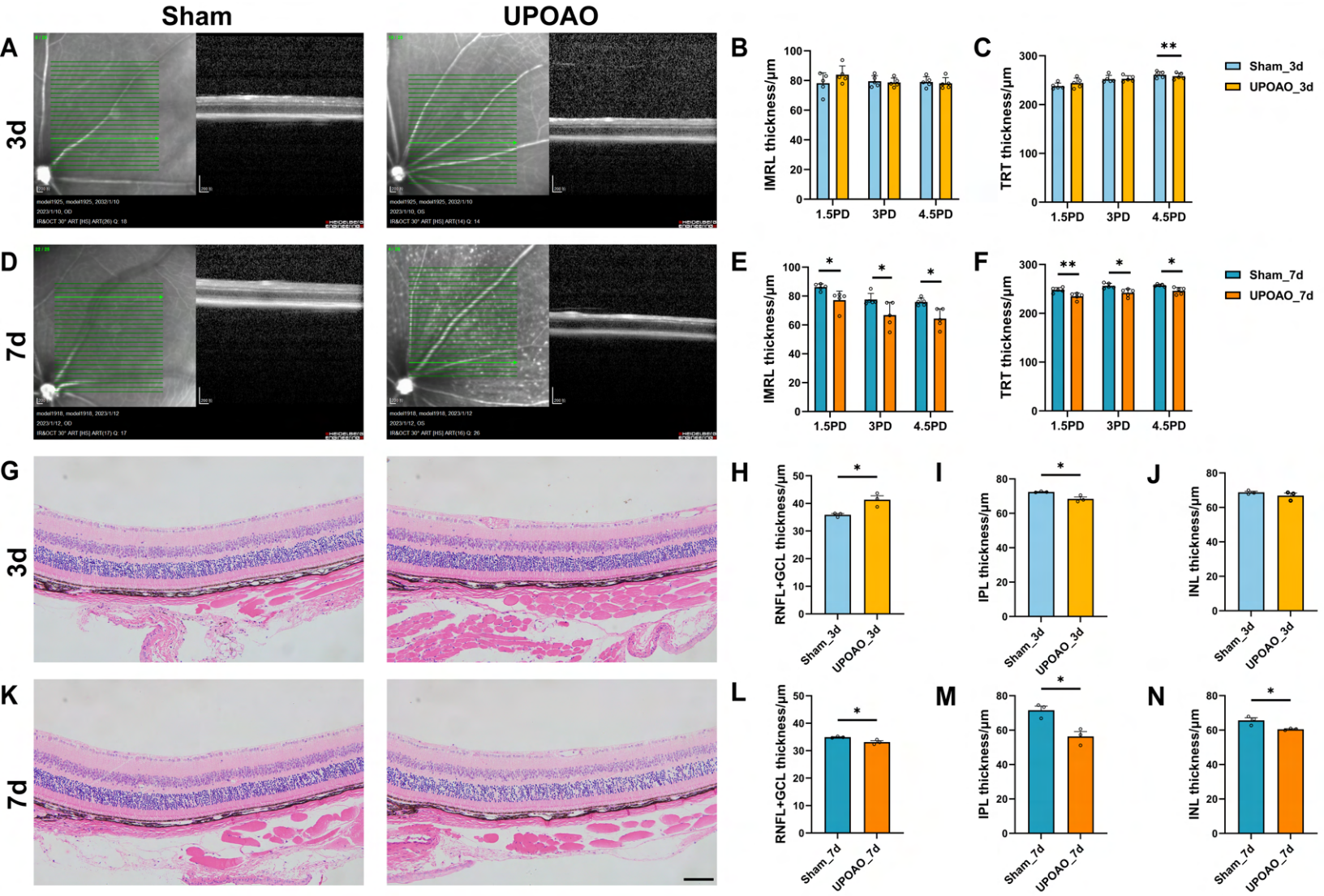
Sham
UPOAO
A
3d
B
IMRL thickness/μm
1.5PD
3PD
4.5PD
C
TRT thickness/μm
**
Sham_3d
UPOAO_3d
D
7d
E
IMRL thickness/μm
*
F
TRT thickness/μm
**
Sham_7d
UPOAO_7d
G
3d
H
RNFL+GCL thickness/μm
I
IPL thickness/μm
J
INL thickness/μm
K
7d
L
RNFL+GCL thickness/μm
M
IPL thickness/μm
N
INL thickness/μm

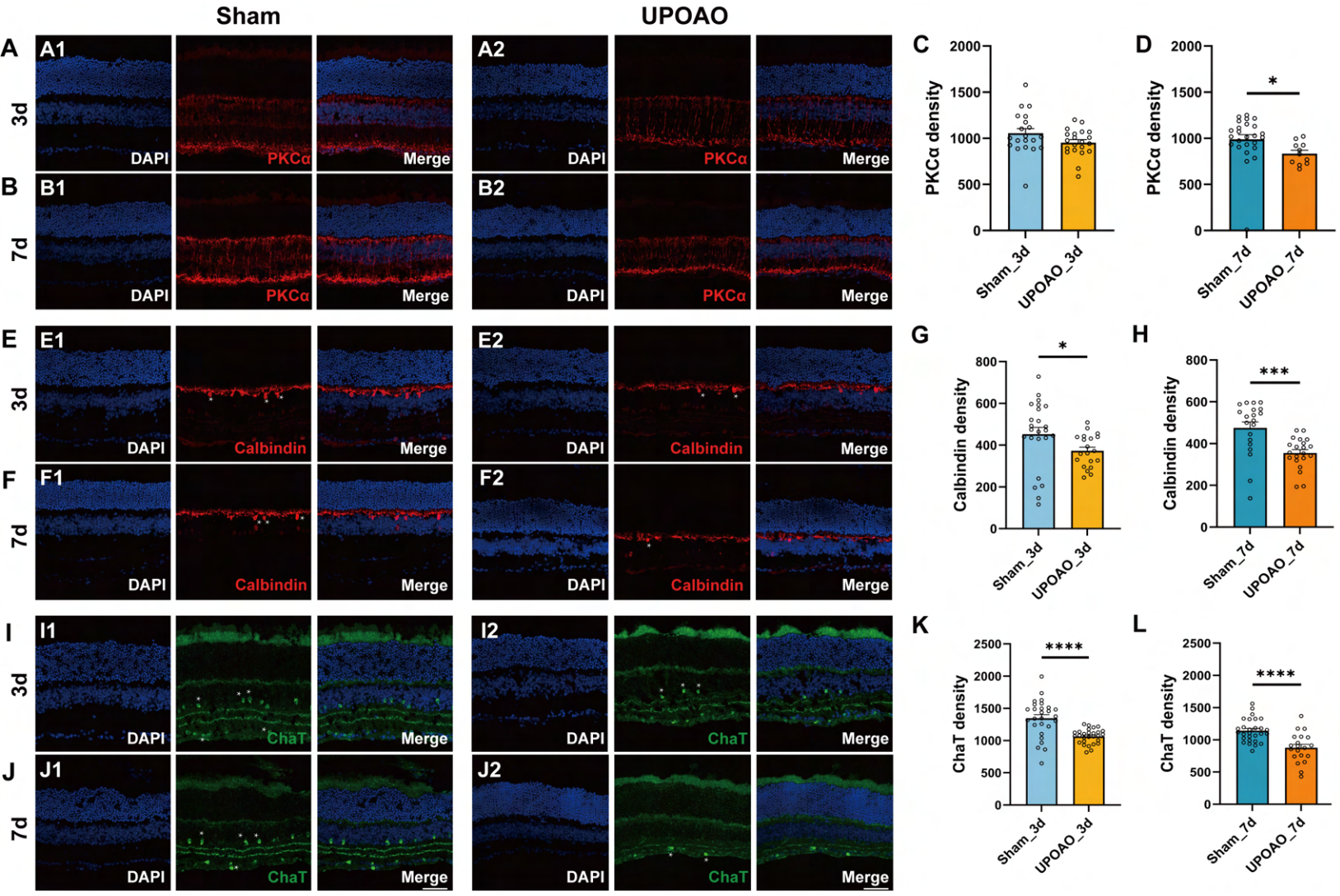
Sham
UPOAO
A
3d
A1
A2
DAPI
PKCα
Merge
B
7d
B1
B2
C
PKCα density
Sham_3d
UPOAO_3d
D
Sham_7d
UPOAO_7d
E
F
Calbindin
G
Calbindin density
H
I
ChaT
J
K
ChaT density
L

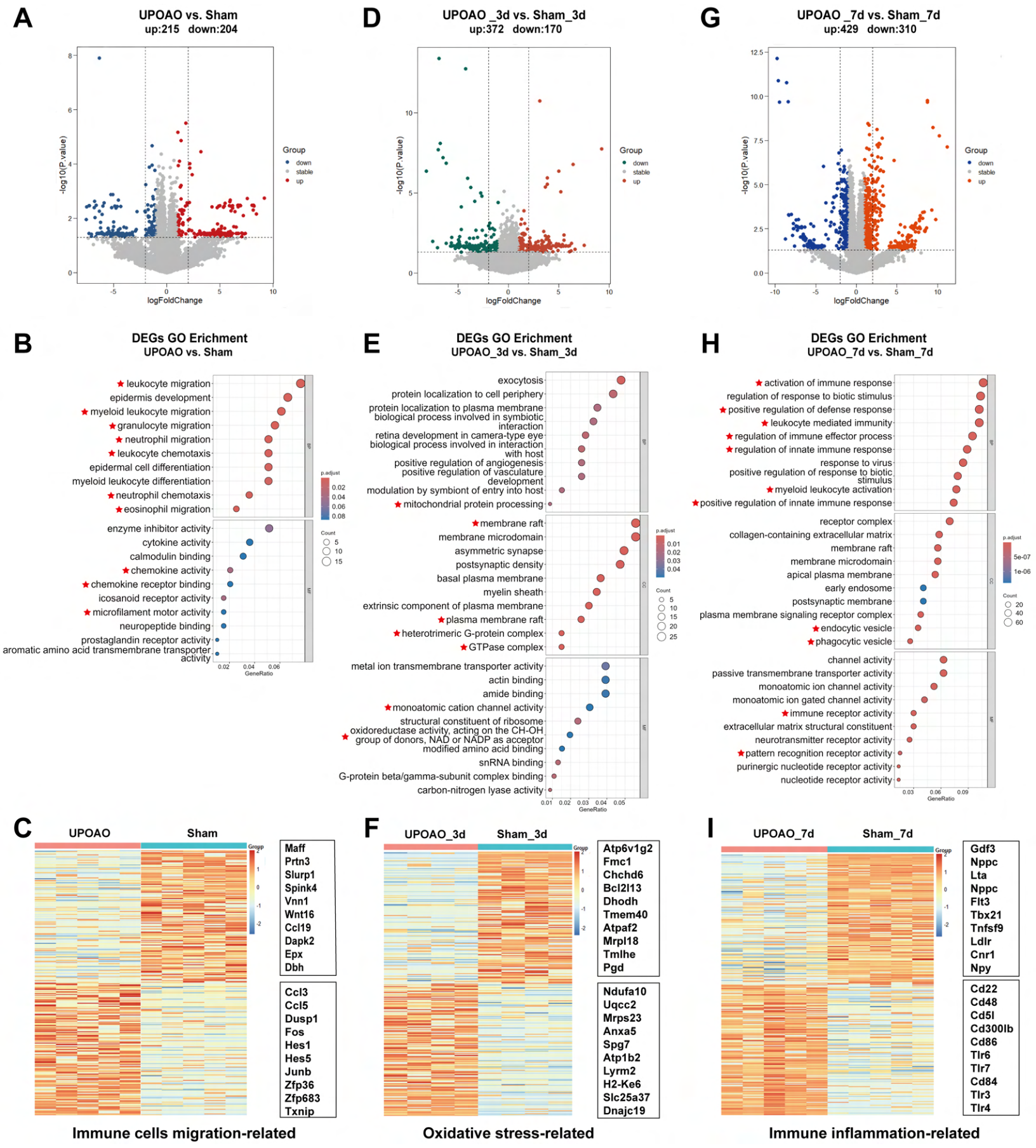
A
UPOAO vs. Sham
up:215 down:204
-log10(P.value)
logFoldChange
Group
down
stable
up
D
UPOAO _3d vs. Sham_3d
up:372 down:170
G
UPOAO _7d vs. Sham_7d
up:429 down:310
B
DEGs GO Erichment
UPOAO vs. Sham
leukocyte migration
epidermis development
myeloid leukocyte migration
granulocyte migration
neutrophil migration
leukocyte chemotaxis
epidermal cell differentiation
myeloid leukocyte differentiation
neutrophil chemotaxis
eosinophil migration
enzyme inhibitor activity
cytokine activity
calmodulin binding
chemokine activity
chemokine receptor binding
icosanoid receptor activity
microfilament motor activity
neuropeptide binding
prostaglandin receptor activity
aromatic amino acid transmembrane transporter activity
GeneRatio
p.adjust
Count
E
DEGs GO Erichment
UPOAO_3d vs. Sham_3d
exocytosis
protein localization to cell periphery
protein localization to plasma membrane
biological process involved in symbiotic interaction
retina development in camera-type eye
biological process involved in interaction with host
positive regulation of angiogenesis
positive regulation of vasculature development
modulation by symbiont of entry into host
mitochondrial protein processing
membrane raft
membrane microdomain
asymmetric synapse
postsynaptic density
basal plasma membrane
myelin sheath
extrinsic component of plasma membrane
plasma membrane raft
heterotrimeric G-protein complex
GTPase complex
metal ion transmembrane transporter activity
actin binding
amide binding
monoatomic cation channel activity
structural constituent of ribosome
oxidoreductase activity, acting on the CH-OH group of donors, NAD or NADP as acceptor
modified amino acid binding
snRNA binding
G-protein beta/gamma-subunit complex binding
carbon-nitrogen lyase activity
H
DEGs GO Erichment
UPOAO_7d vs. Sham_7d
activation of immune response
regulation of response to biotic stimulus
positive regulation of defense response
leukocyte mediated immunity
regulation of immune effector process
regulation of innate immune response
response to virus
positive regulation of response to biotic stimulus
myeloid leukocyte activation
positive regulation of innate immune response
receptor complex
collagen-containing extracellular matrix
membrane raft
membrane microdomain
apical plasma membrane
early endosome
postsynaptic membrane
plasma membrane signaling receptor complex
endocytic vesicle
phagocytic vesicle
channel activity
passive transmembrane transporter activity
monoatomic ion channel activity
monoatomic ion gated channel activity
immune receptor activity
extracellular matrix structural constituent
neurotransmitter receptor activity
pattern recognition receptor activity
purinergic nucleotide receptor activity
nucleotide receptor activity
C
UPOAO
Sham
Maff
Prtn3
Slurp1
Spink4
Vnn1
Wnt16
Ccl19
Dapk2
Epx
Dbh
Ccl3
Ccl5
Dusp1
Fos
Hes1
Hes5
Junb
Zfp36
Zfp683
Txnip
Immune cells migration-related
F
UPOAO_3d
Sham_3d
Atp6v1g2
Fmc1
Chchd6
Bcl2l13
Dhodh
Tmem40
Atpaf2
Mrpl18
Tmlhe
Pgd
Ndufa10
Uqcc2
Mrps23
Anxa5
Spg7
Atp1b2
Lyrm2
H2-Ke6
Slc25a37
Dnajc19
Oxidative stress-related
I
UPOAO_7d
Sham_7d
Gdf3
Nppc
Lta
Nppc
Flt3
Tbx21
Tnfsf9
Ldlr
Cnr1
Npy
Cd22
Cd48
Cd5l
Cd300lb
Cd86
Tlr6
Tlr7
Cd84
Tlr3
Tlr4
Immune inflammation-related

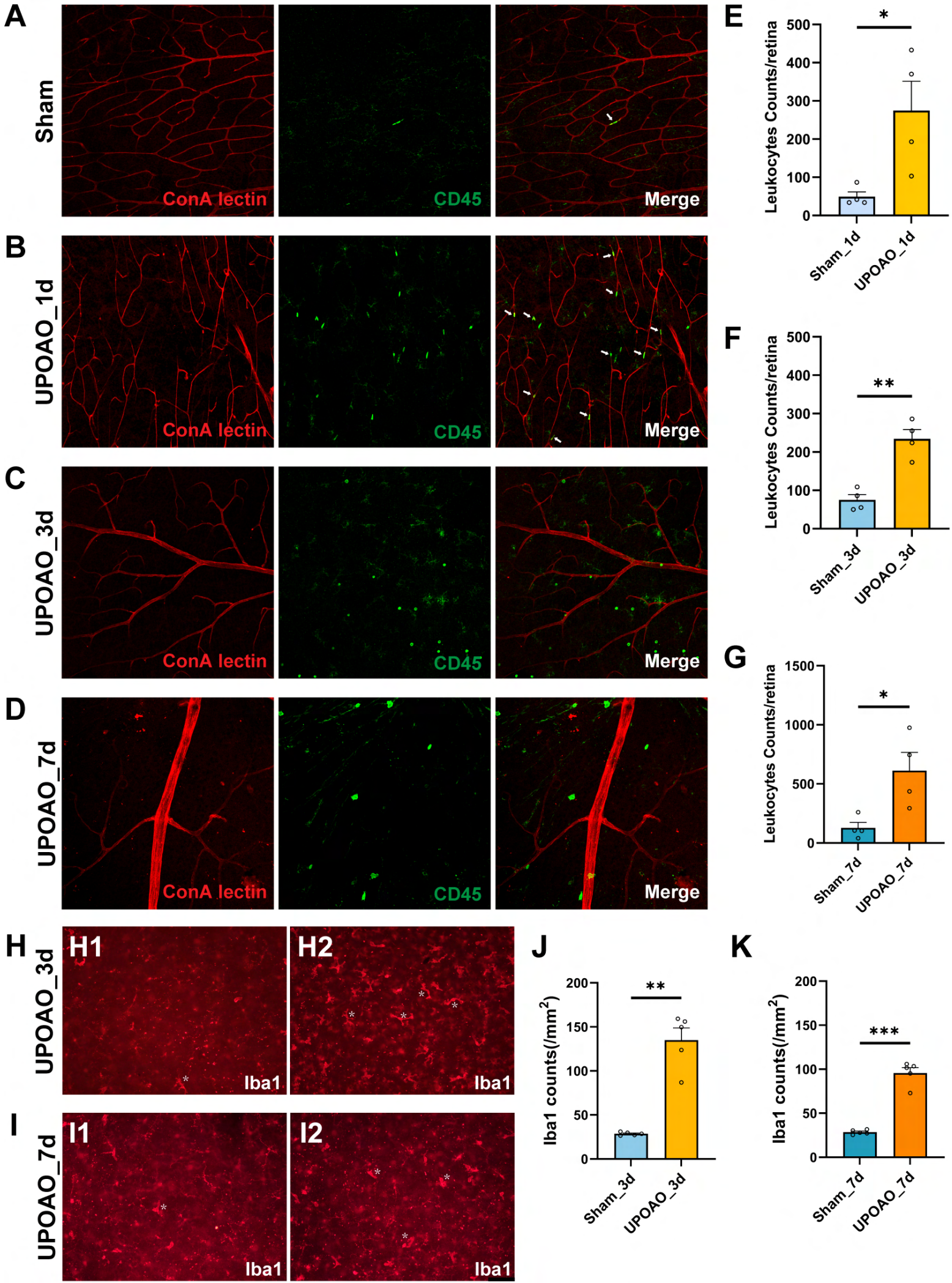
A
Sham
ConA lectin
CD45
Merge
B
UPOAO_1d
ConA lectin
CD45
Merge
C
UPOAO_3d
ConA lectin
CD45
Merge
D
UPOAO_7d
ConA lectin
CD45
Merge
E
Leukocytes Counts/retina
500
400
300
200
100
0
*
Sham_1d
UPOAO_1d
F
Leukocytes Counts/retina
500
400
300
200
100
0
**
Sham_3d
UPOAO_3d
G
Leukocytes Counts/retina
1500
1000
500
0
*
Sham_7d
UPOAO_7d
H
UPOAO_3d
H1
Iba1
H2
Iba1
I
UPOAO_7d
I1
Iba1
I2
Iba1
J
Iba1 counts(/mm2)
200
150
100
50
0
**
Sham_3d
UPOAO_3d
K
Iba1 counts(/mm2)
200
150
100
50
0
***
Sham_7d
UPOAO_7d

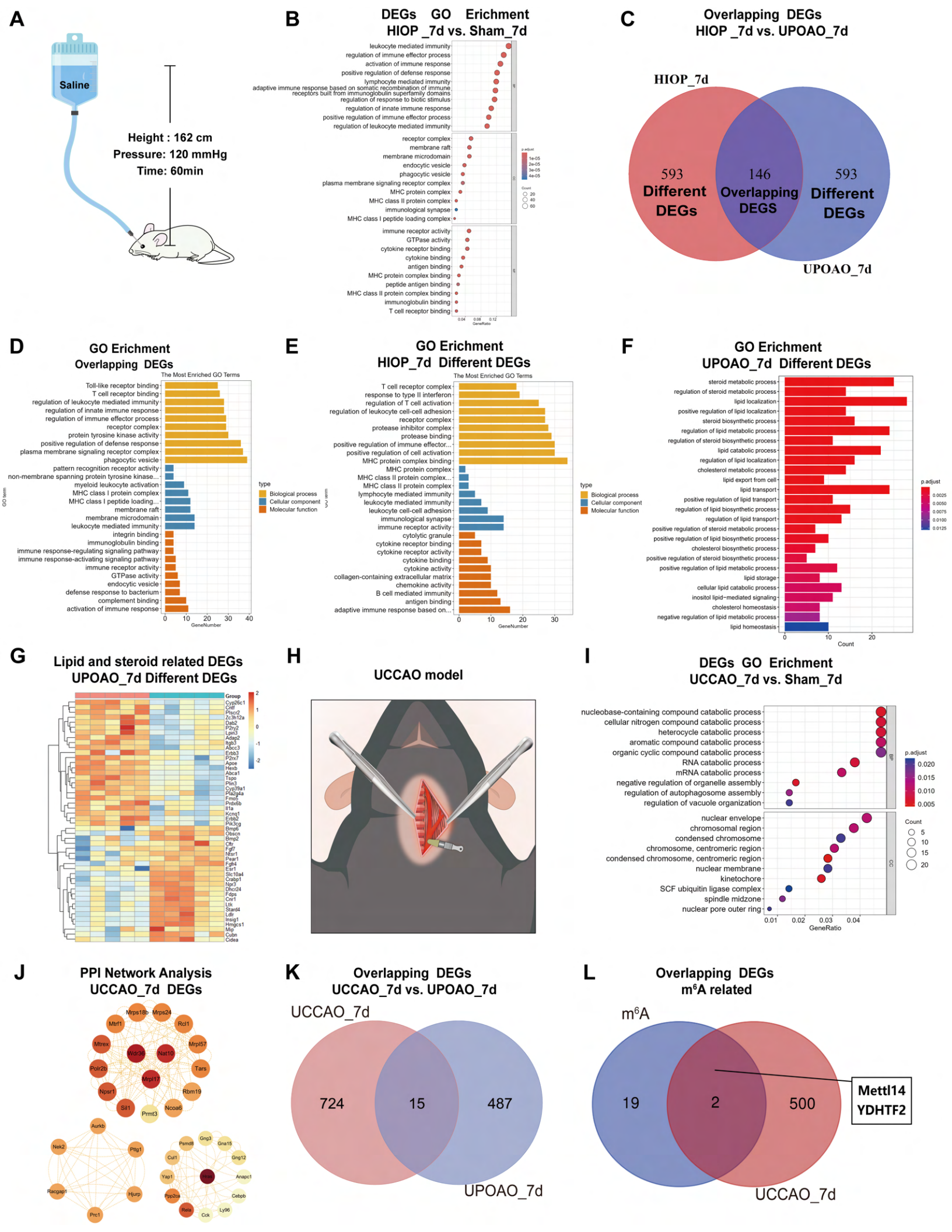
A
Saline
Height : 162 cm
Pressure: 120 mmHg
Time: 60min
B
DEGs GO Erichment
HIOP _7d vs. Sham_7d
leukocyte mediated immunity
regulation of immune effector process
activation of immune response
positive regulation of defense response
lymphocyte mediated immunity
adaptive immune response based on somatic recombination of immune receptors built from immunoglobulin superfamily domains
regulation of response to biotic stimulus
regulation of innate immune response
positive regulation of immune effector process
regulation of leukocyte mediated immunity
receptor complex
membrane raft
membrane microdomain
endocytic vesicle
phagocytic vesicle
plasma membrane signaling receptor complex
MHC protein complex
MHC class II protein complex
immunological synapse
MHC class I peptide loading complex
immune receptor activity
GTPase activity
cytokine receptor binding
cytokine binding
antigen binding
MHC protein complex binding
peptide antigen binding
MHC class II protein complex binding
immunoglobulin binding
T cell receptor binding
GeneRatio
C
Overlapping DEGs
HIOP _7d vs. UPOAO_7d
HIOP_7d
593
Different
DEGs
146
Overlapping
DEGS
593
Different
DEGs
UPOAO_7d
D
GO Erichment
Overlapping DEGs
The Most Enriched GO Terms
Toll-like receptor binding
T cell receptor binding
regulation of leukocyte mediated immunity
regulation of innate immune response
regulation of immune effector process
receptor complex
protein tyrosine kinase activity
positive regulation of defense response
plasma membrane signaling receptor complex
phagocytic vesicle
pattern recognition receptor activity
non-membrane spanning protein tyrosine kinase...
myeloid leukocyte activation
MHC class I protein complex
MHC class I peptide loading...
membrane raft
membrane microdomain
leukocyte mediated immunity
integrin binding
immunoglobulin binding
immune response-regulating signaling pathway
immune response-activating signaling pathway
immune receptor activity
GTPase activity
endocytic vesicle
defense response to bacterium
complement binding
activation of immune response
GO term
GeneNumber
type
Biological process
Cellular component
Molecular function
E
GO Erichment
HIOP_7d Different DEGs
The Most Enriched GO Terms
T cell receptor complex
response to type II interferon
regulation of T cell activation
regulation of leukocyte cell-cell adhesion
receptor complex
protease inhibitor complex
protease binding
positive regulation of immune effector...
positive regulation of cell activation
MHC protein complex binding
MHC protein complex
MHC class II protein complex...
MHC class II protein complex
lymphocyte mediated immunity
leukocyte mediated immunity
leukocyte cell-cell adhesion
immunological synapse
immune receptor activity
cytolytic granule
cytokine receptor binding
cytokine receptor activity
cytokine binding
cytokine activity
collagen-containing extracellular matrix
chemokine activity
B cell mediated immunity
antigen binding
adaptive immune response based on...
GeneNumber
type
Biological process
Cellular component
Molecular function
F
GO Erichment
UPOAO_7d Different DEGs
steroid metabolic process
regulation of steroid metabolic process
lipid localization
positive regulation of lipid localization
steroid biosynthetic process
regulation of lipid metabolic process
regulation of steroid biosynthetic process
lipid catabolic process
regulation of lipid localization
cholesterol metabolic process
lipid export from cell
lipid transport
positive regulation of lipid transport
regulation of lipid biosynthetic process
regulation of lipid transport
positive regulation of steroid metabolic process
positive regulation of lipid biosynthetic process
cholesterol biosynthetic process
positive regulation of steroid biosynthetic process
positive regulation of lipid metabolic process
lipid storage
cellular lipid catabolic process
inositol lipid-mediated signaling
cholesterol homeostasis
negative regulation of lipid metabolic process
lipid homeostasis
Count
p.adjust
G
Lipid and steroid related DEGs
UPOAO_7d Different DEGs
Group
H
UCCAO model
I
DEGs GO Erichment
UCCAO_7d vs. Sham_7d
nucleobase-containing compound catabolic process
cellular nitrogen compound catabolic process
heterocycle catabolic process
aromatic compound catabolic process
organic cyclic compound catabolic process
RNA catabolic process
mRNA catabolic process
negative regulation of organelle assembly
regulation of autophagosome assembly
regulation of vacuole organization
BP
nuclear envelope
chromosomal region
condensed chromosome
chromosome, centromeric region
condensed chromosome, centromeric region
nuclear membrane
kinetochore
SCF ubiquitin ligase complex
spindle midzone
nuclear pore outer ring
CC
GeneRatio
p.adjust
Count
J
PPI Network Analysis
UCCAO_7d DEGs
K
Overlapping DEGs
UCCAO_7d vs. UPOAO_7d
UCCAO_7d
724
15
487
UPOAO_7d
L
Overlapping DEGs
m6A related
m6A
19
2
500
Mettl14
YDHTF2
UCCAO_7d

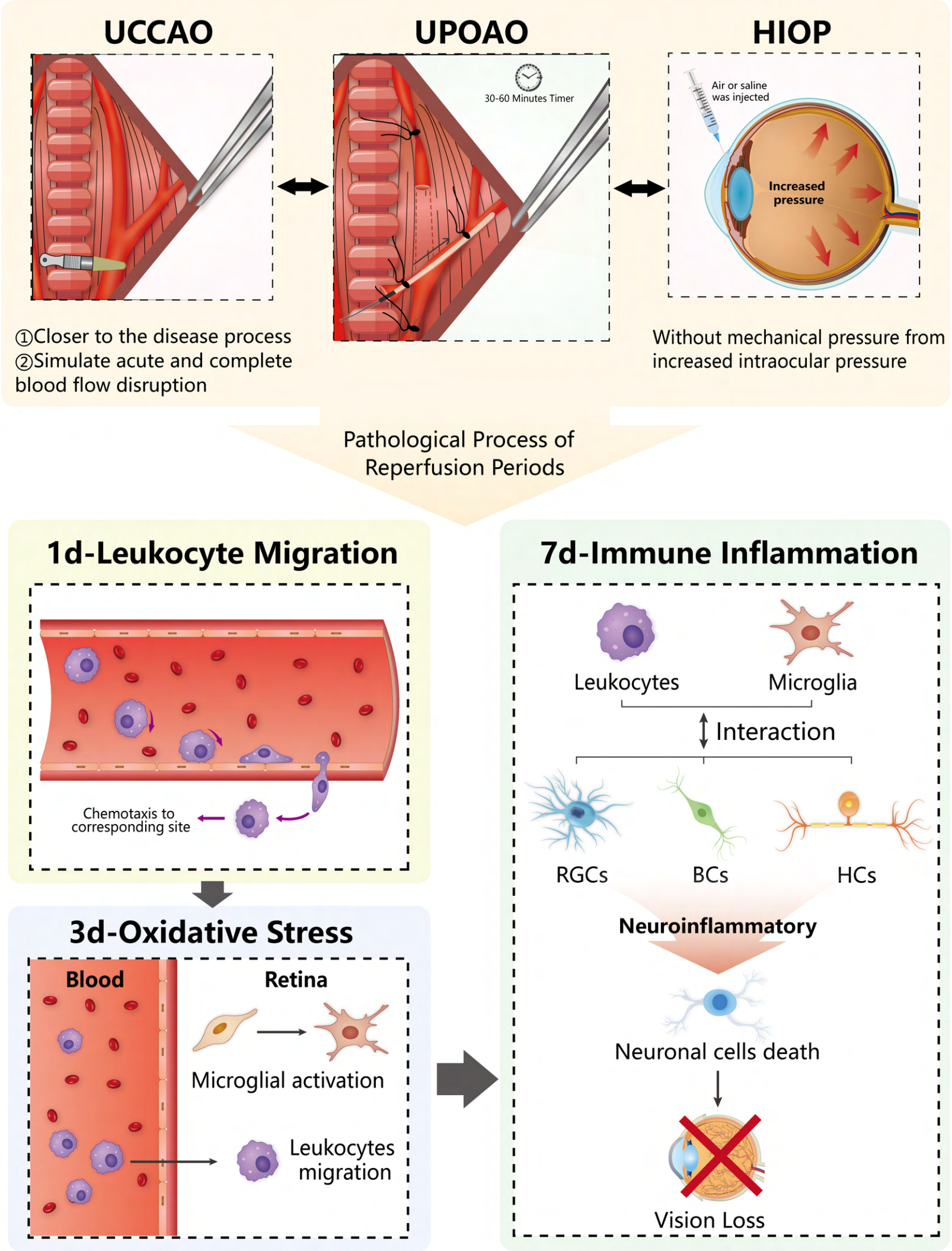
UCCAO
UPOAO
HIOP
30-60 Minutes Timer
Air or saline was injected
Increased pressure
①Closer to the disease process
②Simulate acute and complete blood flow disruption
Without mechanical pressure from increased intraocular pressure
Pathological Process of Reperfusion Periods
1d-Leukocyte Migration
Chemotaxis to corresponding site
3d-Oxidative Stress
Blood
Retina
Microglial activation
Leukocytes migration
7d-Immune Inflammation
Leukocytes
Microglia
Interaction
RGCs
BCs
HCs
Neuroinflammatory
Neuronal cells death
Vision Loss